Titre: Title:	Attrition Resistance of CaO-CuO-Cem Powder for CO2 Capture in Calcium Looping Processes
Auteur: Author:	Peter Asiedu-Boateng
Date:	2015
Type:	Mémoire ou thèse / Dissertation or Thesis
Référence: Citation:	Asiedu-Boateng, P. (2015). Attrition Resistance of CaO-CuO-Cem Powder for CO2 Capture in Calcium Looping Processes [Mémoire de maîtrise, École Polytechnique de Montréal]. PolyPublie. https://publications.polymtl.ca/1734/

UNIVERSITÉ DE MONTRÉAL

ATTRITION RESISTANCE OF CAO-CUO-CEM POWDER FOR CO2 CAPTURE IN CALCIUM LOOPING PROCESSES

PETER ASIEDU-BOATENG
DÉPARTEMENT DE GÉNIE CHIMIQUE
ÉCOLE POLYTECHNIQUE DE MONTRÉAL

MÉMOIRE PRÉSENTÉ EN VUE DE L'OBTENTION
DU DIPLÔME DE MAÎTRISE ÈS SCIENCES APPLIQUÉES
(GÉNIE CHIMIQUE)
AVRIL 2015

UNIVERSITÉ DE MONTRÉAL

ÉCOLE POLYTECHNIQUE DE MONTRÉAL

Ce mémoire intitulé:

ATTRITION RESISTANCE OF CAO-CUO-CEM POWDER FOR CO2 CAPTURE IN CALCIUM LOOPING PROCESSES

présenté par: ASIEDU-BOATENG Peter
en vue de l'obtention du diplôme de: Maîtrise ès sciences appliquées
a été dûment accepté par le jury d'examen constitué de:

M. VIRGILIO Nick, Ph.D., président
M. PATIENCE Gregory S., Ph.D., membre et directeur de recherche
M. LEGROS Robert, Ph.D., membre et codirecteur de recherche
M. SAVADOGO Oumarou, D. d'état, membre

DEDICATION

To my wife Jennifer and kids Adriel and Edeline.,
Thanks for sharing your life with me...

ACKNOWLEDGEMENTS

I had the privilege to work with Prof. Gregory S. Patience who accepted me into his group and encouraged me to succeed even in very challenging times. I will never forget this. I would like to thank my co-supervisor Prof. Robert Legros for his advice and support during this work. Special thanks to Prof. Arturo Macchi of University of Ottawa for his exemplary project leadership and Natural Resources Canada for providing the sorbents. My gratitude also goes to members of my research group especially Dr. Christian Neagoe and Dr. D.C Boffito for their support. Technical staff Daniel Pilon contributed immensely towards the successful completion of this project. Thank you. I would finally like to acknowledge Carbon Management Canada for providing the funding and Natural Resources Canada for supplying the sorbent used in this studies.

RÉSUMÉ

La demande mondiale pour les combustibles fossiles continue d'augmenter, et les préoccupations concernant l'émission de gaz á effet de serre et autres problèmes connexes n'ont jamais été aussi élevées.

La recherche de solutions au réchauffement climatique a reçu l'attention souhaitée et plusieurs technologies ont été développées. L'utilisation de solutions amines en tant qu'absorbant est maintenant disponible au niveau commercial, mais les coûts et les conséquences environnementales en limitent le déploiement. Les cycles à boucle de calcium (carbonate looping, CaL) sont également en développement, mais le recours à une unité de séparation de l'air très onéreuse pour la production d'oxygène pur est nécessaire.

Pour résoudre ces inconvénients, nous suggérons l'utilisation des technologies de solutions amines et des cycles impliquant des composés à base de carbonate de calcium (CaL) à capture de carbone ainsi que les techniques de séquestration.

Canmet Énergie a synthétisé un nouveau sorbant (CaO-CuO-ciment) qui permet d'intégrer les cycles à carbonate (CaL) á la combustion en boucle chimique (chemical looping combustion, CLC) pour l'utilisation dans des réacteurs á lit fluidisé. Ce couplage permet de circonscrire le besoin d'une unité de séparation de l'air. En vue de son utilisation, ce nouveau absorbant doit présenter une excellente tenue mécanique lorsqu'il est fluidisé. L'attrition des particules de l'absorbant survient en raison des collisions entre particules et avec les parois des réacteurs (en particulier dans les régions où des jets à haute vitesse sont présents). Peu d'essais d'attrition sont mentionnés dans la littérature pour des températures de 500 °C. Nous proposons une étude permettant de simuler les conditions causant l'attrition des particules dans des réacteurs á lit fluidisé lors de cycles á calcium, incluant des essais menés à 800 °C. La composition d'un absorbant est critique pour sa tenue mécanique dans de telles conditions. Nous avons mesuré le taux d'attrition pour quatre compositions d'absorbants dans un montage de taille industrielle et comparé celui-ci á celui d'échantillons de calcaire extrait à partir du minerai de cadomin ainsi que deux catalyseurs commerciaux : le pyrophosphate de vanadyle (VPO) et le craquage catalytique fluide(FCC).

Nous avons étudié l'effet de différents paramètres d'exploitation, telle que la vitesse du gaz dans l'orifice comprise entre 180 m s^{-1} to 240 m s^{-1}, la masse volumique du gaz de fluidisation (air, dioxyde de carbone et hélium), la calcination (absorbant calciné 800 °C durant 2 heures) ainsi que la température (23 °C, 500 °C 800 °C). L'effet de la conception du système sur l'attrition a également été analysé, telle que le diamètre de l'orifice (0.39, 0.45 et 0.5 mm)

de même que la composition de l'absorbant.

Dans chacun des essais, un échantillon de 20 g de poudre a été inséré dans un cylindre métallique puis de l'air passe à travers des orifices de dimensions interchangeables : des orifices de 0.39, 0.45 et 0.5 mm forés dans une plaque métallique permettant des vitesses de gaz entre 180 m s^{-1} á 240 m s^{-1} à des températures de 23 °C, 500 °C et 800 °C ont été utilisés.

La vitesse élevée du gaz influence la performance de l'absorbant ainsi que les contraintes mécaniques prédites sur les buses de barboteurs et la plaque de grille dans les réacteurs commerciaux à lit fluidisé. Les fines particules créées par l'attrition sont élutriées sur un tube d'une longueur de de 1.7 m et collectées dans un filtre, puis pesées. Le taux d'attrition du VPO et du FCC à une vitesse de gaz de 180 m s^{-1} sont de 5 et 7 mg h^{-1}, respectivement, alors que ce taux s'élève à 10 mg h^{-1} dans le cas du $CaO_{40}-CuO_{50}-cem_{10}$. Le $CaO_{90}cem_{10}$ présente une résistance à l'attrition 1.3 fois supérieure à celle du $CaO_{40}CuO_{50}cem_{10}$. Ces résultats démontrent qu'un ajout de 10 % de ciment augmente la résistance á l'attrition d'un facteur 1.5 par rapport au calcaire de Cadomin. Dans le cas des essais à des températures de 500 °C et 800 °C, le taux de génération des particules fines pour le $CaO_{40}CuO_{50}Cem_{10}$ n'a augmenté que de 6 %, probablement en raison de l'agglomération de celles-ci. Pour les mêmes températures, le taux de génération des particules fines a quasiment doublé pour le $CaO_{90}Cem_{10}$. Le taux de génération de particules fines varie de façon linéaire avec le débit de gaz et selon le carré du diamètre de l'orifice.

ABSTRACT

The global demand for fossil fuels continues to increase and concerns over emission of greenhouse gases and their associated problems has never been greater. Search for solutions to global warming has received the needed attention and several technologies are under developed. Use of amine based liquid adsorbents are commercially available but cost and environmental consequences limit their frequent deployment. Calcium looping (CaL) is also under development but an expensive air separation unit is required. We need a technology that overcomes deficiencies in the use of amine based and CaL carbon capture and sequestration techniques.

Canmet Energy have synthesized novel sorbent, CaO−CuO−Cem with different compositions based on mass fraction, that integrates calcium looping (CaL) and chemical looping combustion (CLC) for fluidized bed applications with the view to eliminate the air separation unit. The first criterion in accepting this sorbent is to ensure that it does not degrade mechanically during fluidized bed operation due to particle-particle and particle-containing vessel (at high velocity jetting regions) collisions .

Attrition test has been reported at temperature of 500 °C. We present an extensive attrition study that simulates all possible conditions in fluidized bed during calcium looping including tests at 800 °C. A sorbent composition that optimizes attrition resistance is needed. We have measured the attrition resistance of four compostions of the sorbent CaO-CuO-Cem in an industrial scale jet mill and compared them with those of crushed cadomin limestone and two other commercial catalysts: vanadyl pyrophosphate (VPP) and fluid catalytic cracking (FCC).

We studied the effect of orifice gas velocity (180 m s^{-1} to 240 m s^{-1}), fluidizing gas density (air, CO_2 and He), calcination (calcined sorbent for 2 h at 800 °C) and temperature (23 °C, 500 °C and 800 °C). The effect of system design such as orifice diameter (0.39 mm, 0.45 mm and 0.5 mm) as well as sorbent composition have also been investigated.

In each test, we charged 20 g of powder to a metal cylinder and passed air through an interchangeable single orifice of varying diameter: 0.39 mm, 0.41 mm and 0.5 mm drilled through a metal plate. The high velocity gas impinged on the sorbent, which mimicked the expected mechanical stresses at the nozzles of spargers and grid plate in commercial fluidized bed reactors. Attrited fines elutriated through a 1.7 m long tube and collected in a thimble filter. The attrition rates of VPO and FCC at at 23 °C and orifice gas velocity of 180 m s^{-1} were 5 mg h^{-1} and 7 mg h^{-1} respectively; it was 10 mg h^{-1} for the $CaO_{40}-CuO_{50}-Cem_{10}$

sorbent. $CaO_{90}-Cem_{10}$ was 1.3 times more resistant compared with $CaO_{40}-CuO_{50}-Cem_{10}$. These results show that 10 % cement increased attrition resistance of novel sorbent by 50 % as compared with base natural cadomin limestone. Due to agglomeration, rate of fines generation for $CaO_{40}-CuO_{50}-Cem_{10}$ remained essentially constant when temperature was increased from 500 °C to 800 °C. Over the same temperature range of 500 °C to 800 °C, rate of material loss from $CaO_{90}-Cem_{10}$ almost doubled.

TABLE OF CONTENTS

LIST OF TABLES

LIST OF FIGURES

LIST OF SYMBOLS AND ABBREVIATIONS

Abbreviations

CaL	Calcium looping
CCS	Carbon capture and sequestration
CLC	Chemical looping combustion
FCC	Fluid catalytic cracking
MEA	Monoetanolamine
PSD	Particle size distribution
VPP	Vanadyl pyrophosphate

English Letters

cem	cement
K	Attrition rate constant
M	Mass
R_a	Attrition rate
U	Velocity
x	Mass fraction

Greek letters

ρ	density
μ	viscosity
ϕ	sphericity
ξ	voidage
σ	standard deviation

Subscripts

c	cyclone
g	gas
i	particle size class
j	jet
mf	minimum fluidization
o	orifice
p	particle
sv	surface volume

CHAPTER 1 INTRODUCTION

1.1 Background

Global warming, which is due mainly to increasing concentration of atmospheric carbon dioxide has recently gained much attention. The atmospheric carbon dioxide concentration increased by 0.7 % between June 2012 and June 2013 [1]. Almost two-thirds of these increase is related to coal, 22 % to oil and 15 % to natural gas. Fossil fuel will continue to be used well into the current century and the problems associated with global warming will prevail unless mitigation plans are put in place (Fig. 1.1).

Carbon capture and sequestration (CCS) techniques are key option to mitigating CO_2 emissions [2]. Carbon sequestration refer to process of capturing CO_2 from it emission sources whereas carbon storage is method of permanently injecting it deep underground, sea, gas fields, rocks, coal seams and saline aquifers to prevent it from having effect on the environment. Both sequestration and storage can interchangeably refer to injection of CO_2 more than 1 km deep into geological formations. Carbon sequestration reduces green house effect but brings additional operational cost. During storage CO_2 is pumped underground, rise and reach an impermeable cap rock (via buoyancy flow). Storing CO_2 in the sea can form carbonic acid and destroy aquatic life. Underground storage may cause leaks and re-emission into the atmosphere (can be fatal if concentrations exceed 10 %). Well blow-outs can also be catastrophic [2, 3].

Carbon sequestration and storage by mineral carbonation involving the exothermic reaction of CO_2 (in mineral form) with alkaline compounds leads to geological stability and may prevent future leakages. The high energy requirement (350 MW for 100 % storage of emissions from 1.3 GW of coal fired power plant) is its major setback. Mineral carbonation have the capacity to store 20 Mt per annum of CO_2 in the form of $MgCO_3$. Metal organic frameworks (MOFs) with adjustable chemical functionality and high porosity also provide effective means of carbon storage but they still remain remain at laboratory level with additional disadvantage of handling high volumes of chemicals [2].

According to Yang et al [4], reduction in atmospheric CO_2 concentration can be achieved either by cutting down on the use of fossil fuels or by incorporating carbon capture and sequestration technologies. It will be difficult to reduce the use of fossil fuels significantly although efforts are being made to increase the percentage of other sources of energy such as renewable and nuclear. This is due to the fact that fossil fuels contribute 80 % to global

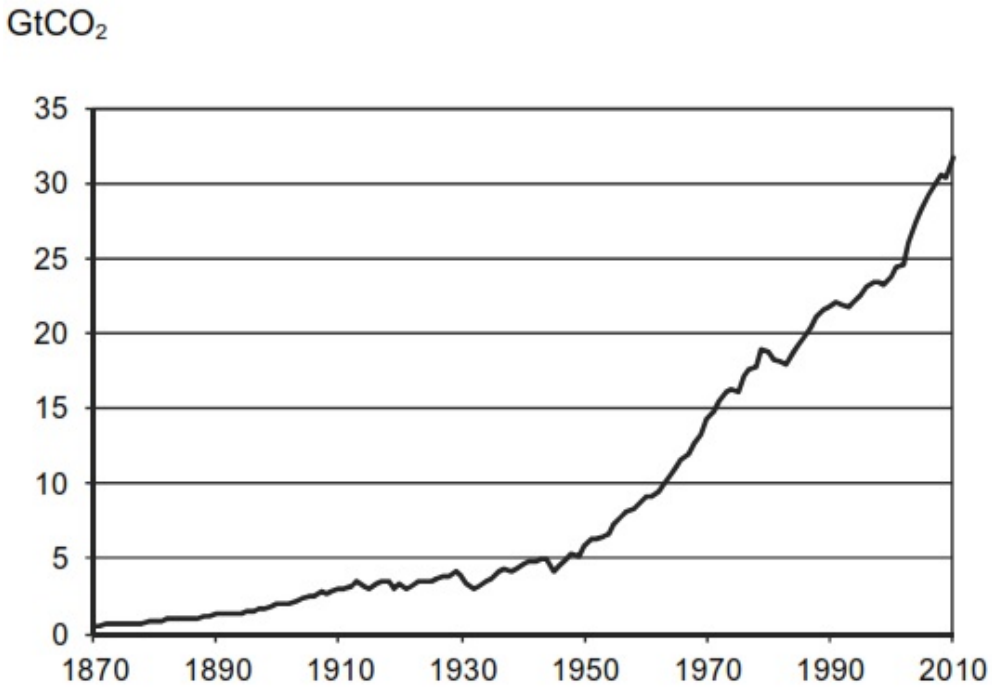

Figure 1.1 Fossil fuel related carbon dioxide emissions trend [1].

energy demand and replacing fossil fuels with nuclear energy will not be feasible in the short to medium terms.

Presently, the only commercially available CCS technology is the low temperature chemisorption of CO_2 using amine based solvents. This involves bringing flue gas containing CO_2 into contact with aqueous monothanolamine (MEA) flowing counter-currently. The CO_2 as a weak base reacts with MEA which is a weak acid to form a water soluble salt. The reaction is reversed in a stripper after treating it thermally to recover the CO_2. Despite the inherent advantages of amine scrubbing such as its applicability even at low concentration and dilute CO_2 system, several disadvantages limit the use of MEA for CO_2 capture. For instance the huge energy requirement of 3.8 GJ/t CO_2 for the CO_2 recovery process since the solvent is heated to 100 °C-120 °C to provide the desorption heat. The solvent must also be heated to the stripper temperature (100 °C-120 °C) during the capture process. Additionally, possible corrosion of process equipment, solvent degradation and the negative impact on the environment renders amine scrubbing unattractive [5, 6].

Membrane separators which capture CO_2 by size exclusion or through affinity for CO_2 are less energy intensive with equivalent amount of CO_2 captured. Frequent material corrosion issues make membranes less attractive. Oxy-combustion CO_2 capture produces 90 % pure CO_2, eliminates NOx but increased SO_2 concentration in exhaust gas leads to corrosion

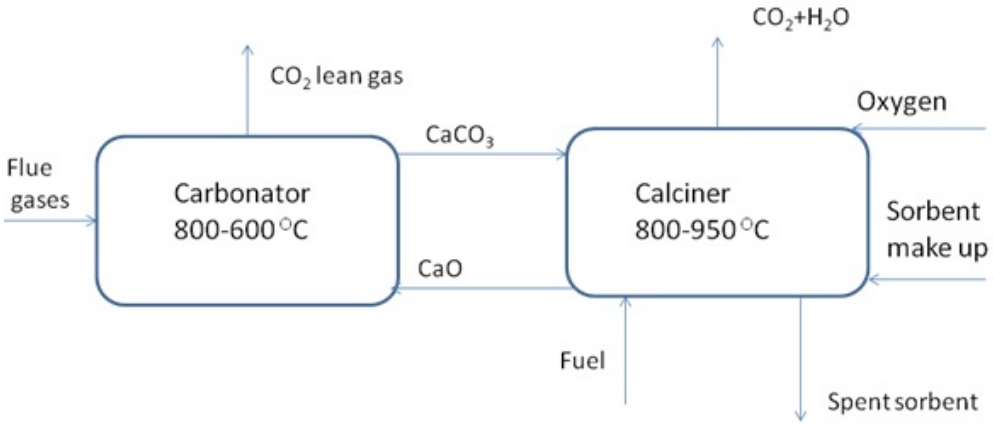

Figure 1.2 Schematic of calcium looping.

problems. Membrane and CO_2/O_2 techniques are promising but they not yet mature for industrial applications [3].

The cost of capture step in CCS is the highest (USD15-75/t of CO_2 captured) compared to transportation (USD 1-8/t CO_2 captured) and storage (USD 0.5-8/t CO_2 captured) [1]. The high cost of CCS and the demerits associated with MEA have led to the search for more cost and environmentally effective alternative technologies for CO_2 capture. Towards this end, the use of solid sorbents especially calcium oxide in carbonation-calcination reactions, have gained prominence as potential CCS technology [7, 8] with possibility of capturing CO_2 with better process economics and energy efficiency [8, 9, 10]. The average cost of MEA capture is (USD 50/t CO_2 captured) which is equivalent to 0.03 \$/kWh [5, 6] but Abanades et al [8] showed that with Ca-based sorbents cost of CO_2 capture can be as low as (USD 15/t CO_2 captured) translating into 0.0075 \$/kWh mainly because of the power generated by the capture system.

Calcium oxide (abundant and inexpensive limestone which is cheaply abundant) reacts with CO_2 -rich flue gas typically at a temperature of 600 °C in carbonation reaction (I) as illustrated in Fig.1.2

$$CaO_s + CO_2 \longrightarrow CaCO_3 \qquad \text{(I)}$$

The reverse calcination reaction, which usually occurs at temperatures above 800 °C (depending on the equilibrium) separates CO_2 for subsequent compression and geological storage. The regenerated sorbent is returned to the carbonator to begin another cycle [1]. The cost

of calcium looping (CaL) process is usually high due to the expensive air separation unit [12, 13, 14]. Moreover, regenerating the sorbent at high temperature during oxy-fuel combustion sinters and leads to reduction in sorbent activity to capture CO_2. Burning solid fuels (which contain SO_2) will reduce the performance of the solid sorbent. Oxy-fuel combustion usually results in corrosive CO_2 stream. This situation makes CO_2 unsuitable for transport by pipelines. However, simulations conducted on experimental data in [9, 10] show that high temperature CCS with solid sorbents can lower the cost compared with low temperature MEA. The cost effectiveness and energy efficiency of calcium looping (CaL) can further be enhanced when integrated with chemical looping combustion (CLC) utilising oxygen carriers such as copper with aim of averting problems associated with individual technologies and producing electricity (Fig.1.3).

Chemical looping combustion operates with two interconnected reactors: fuel reactor and air reactor (Fig. 1.4). A metal oxide which serves as a source of oxygen circulates between these reactors and combustion process is separated into oxidation and reduction reactions [13]. Oxidation of the fuel takes place in the fuel reactor and produces CO_2 and water vapour (reaction II). The reduced form of the metal oxide is re-oxidized in the air reactor (reaction III) and returned to the fuel reactor to begin another cycle.

$$(2\,\mathrm{n} + \mathrm{m})\mathrm{Me_yO_x} + \mathrm{C_nH_{2m}} \longrightarrow (2\,\mathrm{n} + \mathrm{m})\mathrm{Me_yO_{(x\text{-}1)}} + \mathrm{mH_2O} + \mathrm{nCO_2} \qquad \text{(II)}$$

$$\mathrm{Me_yO_{(y\text{-}1)}} + \tfrac{1}{2}\mathrm{O_2} \longrightarrow \mathrm{Me_yO_y} \qquad \text{(III)}$$

Pure CO_2 is obtained after condensing the water vapour. This eliminates the need for extra energy intensive air separation system and thus improves the economics of the process [3, 13, 14]. The heat of reaction remains unchanged compared with combustion in which both air and fuel contact with each other directly.

The efficiency of CLC is dependent on the choice of oxygen carrier. Oxides of transition metals such as Cu, Ni, Fe, Co and Mn are effective. Selection criteria of oxygen include fluidizability, stability and reversibility during reduction-oxidation reactions, attrition resistance and tendency agglomeration resistances (for fluidized bed applications) etc. Environmental and health issues as well as material availability and cost are also considered. The oxygen carrier determines the heat distribution between the interconnecting reactors. Exothermic reduction reactions by oxygen carriers are the basic condition that must be met for it to be applied in an integrated CaL-CLC. In the calciner (fuel reactor), the energy released during the exothermic reduction of the oxygen carrier is used to decompose the $CaCO_3$. Cho et

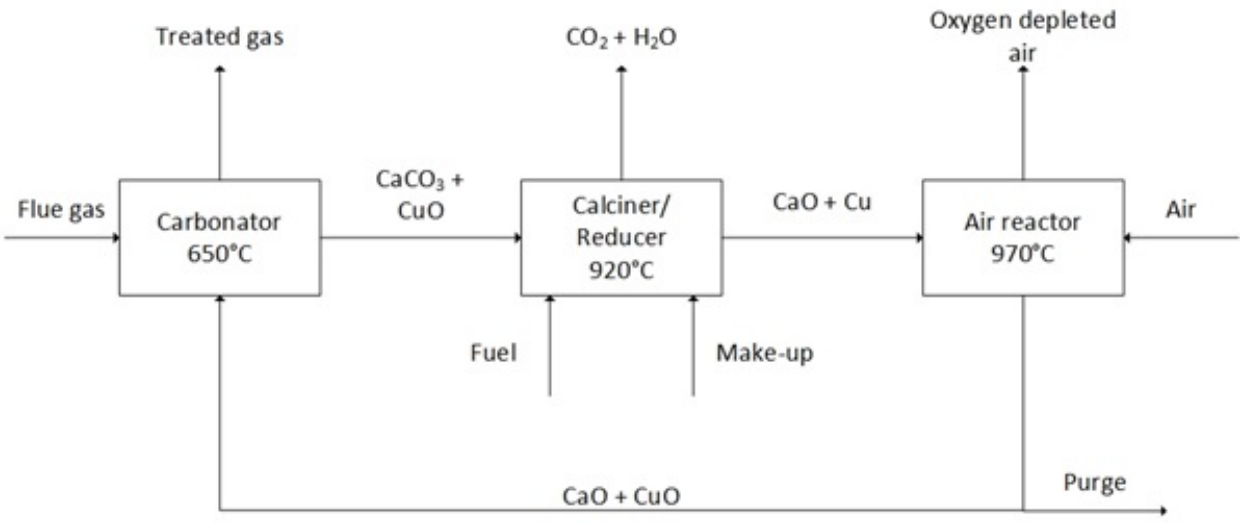

Figure 1.3 Schematic of integrated CaL-CLC system.

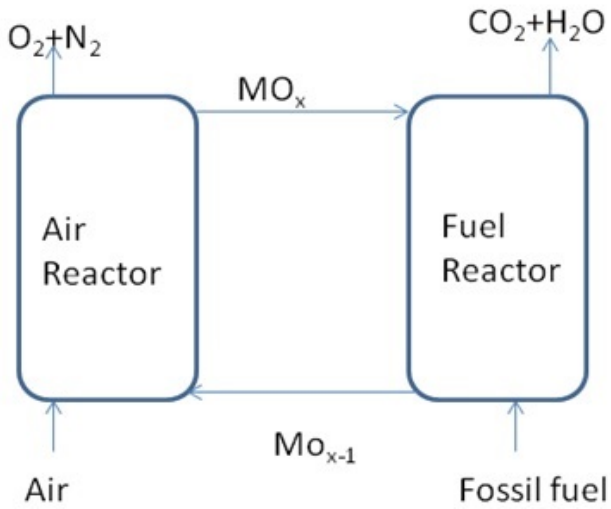

Figure 1.4 Schematic of chemical looping combustion.

al [14] compared the properties of many transition metals oxides and concluded that nickel based oxygen carrier are the most promising. Contributions from [16, 17] indicate that copper based oxygen carriers are exothermic during reduction reactions thus avoiding the need for energy supply.

Manganese oxides can be used since they undergo exothermic reduction reactions [16]. However only Mn_3O_4/MnO cycles can be used at 600 °C to 800 °C and 800 °C to 950 °C (typical CaL-CLC conditions) and reaction with CH_4 is endothermic. The critical parameter for selection of oxygen carrier is the specific heat of reduction (Table 1.1) to generate energy; and CuO is the best since it has the highest specific heat of reduction with CH_4. Copper, however, suffers agglomeration and sinters above 950 °C blocking lattice sites as well as substantial reduction in reactivity as the number of cycles increases. The energy released from reduction of CuO with gaseous fuels such as CH_4 is used to decompose $CaCO_3$. Both the carbonation (reaction I) and oxidation (reaction IV) of copper are exothermic and the heat released can be used to generate electricity [18].

$$2\,Cu_s + O_{(2g)} \longrightarrow 2\,CuO_s \qquad \text{(IV)}$$
$$4\,CuO_s + CH_{4(g)} \longrightarrow 4\,Cu_s + 2\,H_2O + CO_2 \qquad \text{(V)}$$

Fluidized beds are the reactors of choice for practical implementation of CaL since they provide effective means of contacting gas and solids and offer good means of heat and mass transfer [19]. A number of studies have been conducted with focus on bubbling beds [19, 20] and circulating fluidized beds [21, 22]. High fluid velocities in these reactors (depending on the operating regime) usually cause solid particles to collide at high frequency with each other and with walls of the containing vessel. Momentum transfer during collision leads to particle attrition (mechanical degradation).

Sorbent attrition produces fine particles that can be elutriated and must be replenished. Attrition is an undesirable phenomena especially with sorbents containing expensive and toxic copper oxide as it results environmental and health concerns and icreases operational cost. In an effort to finding a cost effective and energy efficient CCS technology, Canmet Energy is developing novel sorbents that integrates CaL and CLC [12, 23]. Testing the attrition resistance of the novel sorbent is the first critical undertaking in commercialising this technology together with fluidized bed carbonation/calcination cycles test of reactivity.

Table 1.1 Choice of oxygen carrier for CH_4 fuel in CLC [16]

Oxygen carrier	Heat of reaction, kJ/mol	Specific heat, kJ/kg.
CuO-Cu	-211.6	0.66
Cu_2O-Cu	-139.9	0.24
NiO−Ni	-83.5	0.58
$Mn_2O_3-MnO_4$	-446.3	0.24
Mn_2O_4-MnO	-92.2	0.41
Co_3O_4-CoO	-30.3	0.03

1.2 Problem Statements

1. High fluid velocities in fluidized beds cause high frequency sorbent particle-particle and sorbent particle-reactor wall collisions. This results in momentum transfer between particles leading to mechanical degradation (attrition) of sorbent particles, production of fine particles and subsequent elutriation of fines.

2. High temperature requirement in calcium looping-chemical looping combustion may agglomerate and sinter sorbent and reduce sorbent reactivity performance.

3. Reduction in the mechanical and reactivity performance of sorbents require the addition of fresh sorbent. This increases the operational cost of calcium looping processes.

1.3 Objective

1.3.1 Main objective

As part of development of CCS technology by Carbon Management Canada, the main objective of this thesis is to test the attrition resistance of novel sorbent for post-combustion CO_2 capture and ascertain its suitability for fluidized bed operations.

1.3.2 Specific objectives

The main objective of this thesis has been divided into three sub-objectives:

1. Establish an attrition test protocol that is valid for commercial CaL-CLC operations.

2. Determine the effect of operating conditions such as temperature, orifice gas velocity, gas density and duration of test as well as effect of orifice diameter on the attrition resistance of the sorbent.

3. Identify sorbent composition that maximizes attrition resistance.

The novelty of this work relates to operating the attrition mill at 800 °C, which has never been done before.

This study determines the attrition resistance of Ca-based aluminate cement bound sorbent with four compositions in a jet mill and compares them with crushed cadomin limestone and two other commercial catalysts: DuPont's vanadium pyrophosphate (VPP) and fluid catalytic cracking (FCC).

The sorbent prepared by Canmet Energy, contains varying amounts of calcium aluminate cement as binder aimed at optimising its attrition resistance. We conduct test at temperatures up to 800 °C using an industrial jet attrition mill that was employed by DuPont during the development of VPP catalyst. The testing condition simulate industrial fluidized bed reactors to be employed during the commercialization of this technology. The results of this study can, therefore, guarantee the expected attrition issues or otherwise in real calcium looping process as it will incorporate effects of both material properties as well as process conditions and system design.

CHAPTER 2 LITERATURE REVIEW

2.1 Sorbent attrition

In a fluidized bed reactor, the bed is most of the time in a rigorous motion and this usually results in high frequency particle-particle and particle-wall collisions. Collision leads to mechanical degradation of bed material. Particles surfaces are abraded or the entire particle could fragment.

The possible elutriation of attrition generated fines can have serious implications on safely of equipment, personnel, environment and operational cost. Fine particles of materials with toxic compounds leads to health and environmental issues. Wear of containment vessels and system contamination may also occur as result of attrition. If fine material builds up in systems, it may lead to an explosion. Elutriation of material from reactors means that it must be regularly replenished which creates additional material cost and may render the entire process economically unattractive [24]. Attrition changes the particle size distribution in a reactor during operation and affect the hydrodynamics, reaction rate, heat and mass transfer [25, 26]. Most attrition tests focused only on material properties to determine the attrition resistance [27]. A complete attrition test must account for process conditions and system design as well. Vaux and Kaeairins [28] investigated the effect of thermal stress, chemical stress and mechanical stress on sorbents and found that each of these process factors have significant effect on materials attrition resistance. Material properties such as particle size distribution, surface structure, and shape can seriously influence its attrition resistance. Attrition test must consider conditions such as gas and solids velocity, solids residence time, system temperature and pressure. Orifice diameter, grid type, wall hardness are the main design variables [29]. Studying attrition enables one to understand the mechanism and find a suitable model to predict the extent of anticipated attrition of sorbents [30] and efficient design of fluidised bed reactors [31].

2.2 Mechanisms of attrition

During abrasion (Fig. 2.1) asperities on surfaces of particles are chipped off leading to more rounded and large number of finer particles (narrow size distribution). The particle size distribution becomes bimodal as compared with the original unimodal particle distribution. Particles abrasion occurs easily as it requires just a minimum threshold energy. The particle size distributions of the parent particles do not change significantly. In fragmentation, the

particle breaks into a large number daughter particles usually of the same order of magnitude as the parent particle. The results of particle fragmentation is a wider particle size distribution compared to the parent particles [29, 30].

2.3 Assessment of attrition

Several factors have to be considered in order to measure the attrition resistance of a material. Individual particles or group of particles can be used to assess attrition in a wide range of methods based on a variety of empirical indices [32]. Attrition resistance of a material can be determined in terms of materials loss or changes in particle size distribution when it subjected to specific stress. Gwyn [33] estimated the generation of fines with time and stated that attrition rate increase with time. Epstein [34] developed a method that measured the degree of fragmentation based on two functions: probability of solid to fragment with a time interval and fraction of fragmented products with a particular size range.

2.4 Grindability indices

2.4.1 Attrition rate

Attrition rate (R_a) is defined in terms of the fractional reduction in mass (M) of material with time due to elutriation of generated fines (Eq. 2.1 and 2.2). This is the usual method of assessing the attrition resistance of a material in fluidized bed operations. Reduction in the mass of bed material or mass of entrained and subsequently elutriated fines generated is measured [35].

$$R_{\mathrm{aj}} = -\frac{1}{m}\frac{dm_e}{dt} \tag{2.1}$$

$$R_{\mathrm{aj}} = \frac{dm_e}{dt} \tag{2.2}$$

However, depending on the available resources and data required, different authors have defined attrition rate (Equation 2.3) based on changes in the particle size distribution [36].

$$R_{\mathrm{aj}} = -\frac{1}{d_o}\frac{dd_N}{dt} \tag{2.3}$$

where d_o and (d_N) are particle median diameters at the start of a test and after N cycles respectively.

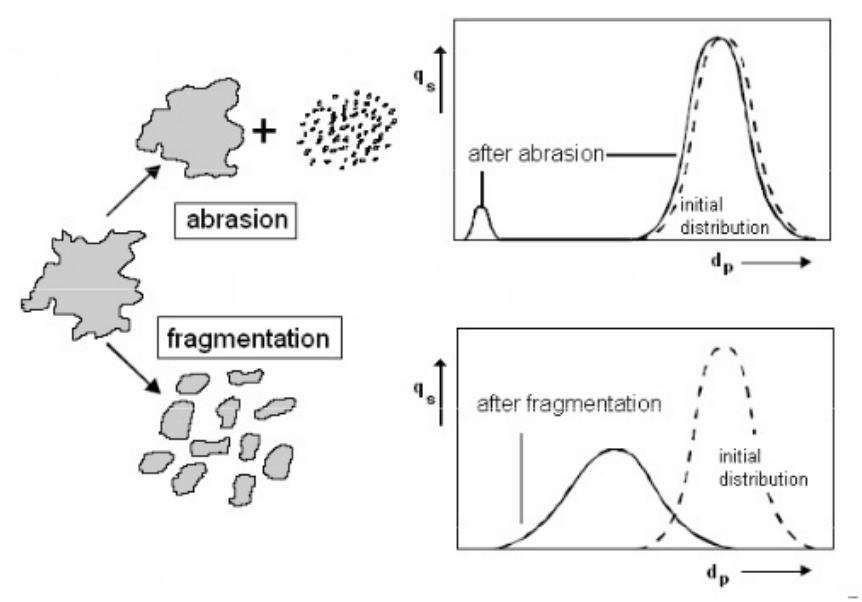

Figure 2.1 : Modes of Attrition [29]

.

Based on production of fines greater than 325 mesh (44 µm), Forsythe and Hertwig [37] gave the attrition rate as a percentage per hour (Eq. 2.4).

$$R_{\mathrm{a}} = \frac{(\%\ of - 325\ mesh\ at\ start - (\%\ of - 325\ mesh\ after\ 1h)}{(\%\ of - 325\ mesh\ at\ start)} X100\ \%/h \tag{2.4}$$

Equation 2.4 is applies to just a specific size class of particles and 1 h test duration. Moreover, it does not consider fines that are kept in the attrition zone as these have an effect on the friability of the material.

Gwyn [33] improved on the work of Forsythe and Hertwig, and estimated the attrition rate with mass-time relation (Eq. 2.5). Gwyn's equation later gave birth to the ASTM D5757 method.

$$R_{\mathrm{aj}} = kt^m \tag{2.5}$$

where m is lies between 0.43 - 0.9, t is time and k is an attrition constant which decreases with particle size and is valid for only size distribution [38]. Gwyn's relationship indicates that attrition increases with time. This is only true when steady state attrition rate is not attained. Attrition rate is dependent to a large extent on the conditions of elutriation in the test apparatus.

2.4.2 Attrition index

The ASTM D5757-11 standard [39] uses percent fines at five hours of operation to evaluate the attrition index [Eq. 2.6] with particles in the 10 µm to 180 µm range of fluid catalytic cracking catalyst. Eq. 2.6 calculates the attrition rate as the fraction of fines collected to total mass charged to the mill. The test duration is 5 h. The first 5 h of operation may only give an indication of the initial attrition. The test must be extended to include the attrition rate under steady state conditions. The particle size range contains fines which can easily be elutriated and may increase the recorded the attrition rate. Several suggestions were given to improve on the ASTM method in [40].

$$R_{\mathrm{aj}} = -\frac{(M_1 - M_o) + (M_5 - M_e)}{M_s} X100\% \tag{2.6}$$

M_o = mass of empty fines collection system at start of test.
M_1= mass of fines collection system after 1 h. Mass of collection system and fines collected during the first 1 h.
M_e = mass of second empty fines collection system. This installed after 1 h to collect the fines.
M_5 = mass of second fines collection system after 5 h. Mass of collection system and fines collected during the last 4 h.
M_s = mass of sample.

2.4.3 Hardgrove index (HDI)

This is based on newly produced surfaces during size reduction process of material sample of nearly equally sized particles. The new surface produced is compared as a percentage with that of a standard coal. The ASTM standard D409/D409M-12 [41] calculates the value of the index according to equation (2.7)

$$HGI = 6.7M + 10.63 \tag{2.7}$$

where M = mass of 75 µm (No 200) mesh material. The fines are produced during 60 revolutions of material with particles between 590 µm to 1190 µm in ball-ring pulveriser. Only relative hardness values are obtained since the mill is calibrated with coal which is assigned a hardness value of 100.

2.4.4 Work index

Work index is the kWh needed to mill 900 kg of material from an large particle size until 80 % of the particles are less than 100 µm. This can be calculated with (Eq. 2.8) [42]. Large quantity of test material needed limits its applicability to large scale operations.

$$W_{\mathrm{i}} = \frac{44.5}{P_t^{0.23} \times G_e^{0.83} (\frac{10}{P_{80}{}^{0.5}} - \frac{10}{F_{80}^{0.5}})} \tag{2.8}$$

P_t = size of test sample, G_e = grindability (g/rev), P_{80}= product size(1 µm), F_{80} = feed size (1 µm).

2.5 Attrition testing

Attrition tests may be carried out using any of the several experimental processes including ASTM-D5757 by air jet [39], jet cup [43], fluidised beds [44] and cyclonic [45, 46]. These test methods suggest that there is no universal method for assessing the attritability of a powder. Ranking the relative attrition resistance of different materials after subjecting each to different stresses can lead to conflicting results. According to [47]

> "If we took a batch of rubbers and a batch of diamonds, and rubbed them on abrasive paper, we would conclude that the diamonds were more attrition resistant. If we instead struck the particles with a hammer we would conclude that the rubber were more attrition resistant".

The method to be used in testing attrition resistance should simulate the real situation and stress to be experience in commercial processes.

2.5.1 Jet mill attrition testing

The jetting region of a fluidized bed is a major source of attrition. The jet attrition test method mimics catalyst attrition in the jetting region of distributor in a fluidised bed reactor. This involves introducing gas through an orifice at high velocity to impinge on sorbent (Fig.2.2). The powder particles collide at high frequency leading to mechanical degradation. The fines generated are entrained in the gas and entrainment rate remains constant and independent of particle diameter after reaching saturation stage.

Contractor et al [48] measured the attrition resistance of catalyst in jet mill during the development of DuPont's butane oxidation process. Patience and Bockrath [49] employed

a jet mill to measure the attrition resistance of powder. An attrition rate of $4\,\mathrm{mg\,h^{-1}}$ was achieved when an orifice velocity of $210\,\mathrm{m\,s^{-1}}$ passed through a 0.4 mm orifice. The high attrition resistance was attributed to heat treatment in the spray dryer that gave higher catalyst bulk density. The attrition resistance of limestone from 0.5 h to 144 h has been measured in jet apparatus [50]. A model with an exponential function was developed to characterise the attrition process. The fines generation rate was inversely proportional to the particle volume for the initial and stable stages. The effect of attrition resistance of catalyst in an acrolein process was tested with an air jet apparatus with a 0.4 mm orifice in [51]. The concentration of the salt was higher in the attrited fines than the catalyst in the mill. The extent and pattern of limestone attrition by surface wear in the dense phase fluidised bed has been studied [52]. Attrition of particles caused by impact was dependent on impact velocity. Limestone particle attritions under oxyfiring condition have been investigated with similar procedure as in[53]. The attrition behaviour of CaO nanoparticles has been investigated with an air jet apparatus under high temperature and ordinary conditions. Results showed that $Ca_{12}Al_{44}O_{13}$ formed under calcination conditions. Attrition resistance increased with Ca/Al ratio and attrition mainly occurred in the region of CaO particles [55].

Larger initial particles experienced higher attrition rates because they possessed greater entropy (measure of disorderliness in particle size) and higher chance of being involved in collisions [55]. Disordered particle size resulted in higher frequency of attrition-causing collisions. Mechanism of limestone attrition in jet mill was investigated in [30] for different particle size ranges. Abrasion was the main mechanism for particles of size 710 µm to 850 µm in diameter but it changed to total fragmentation as the size decreased below 180 µm. Werther and Xi [56] studied the mechanism of jet induced attrition with a Gywn type of apparatus and proposed a model (Eq. 2.9) for the attrition rate. They related the surface energy created with the energy spent. Where K_j is material specific attrition constant, ρ_g is gas density, d_o is orifice diameter, U_o is orifice gas velocity.

$$R_{\mathrm{aj}} = n_0 k_j \rho_g d_p d_O^2 U_O^3 \tag{2.9}$$

Catalyst attrition is much greater at high orifice velocities and larger orifice diameter due to increased mass flowrate which induce higher frequency of collisions. ASTM D5757[39] is the most common testing method with a high gas velocity through the orifice and much reduced velocity in the bed. Thus it takes long a time to attrit the catalyst. Ghadiri et al[57] established a more general relation for attrition rates of FCC catalyst using single particle impact in the jetting region of fluidised bed and predicted 3.31 for the exponent.

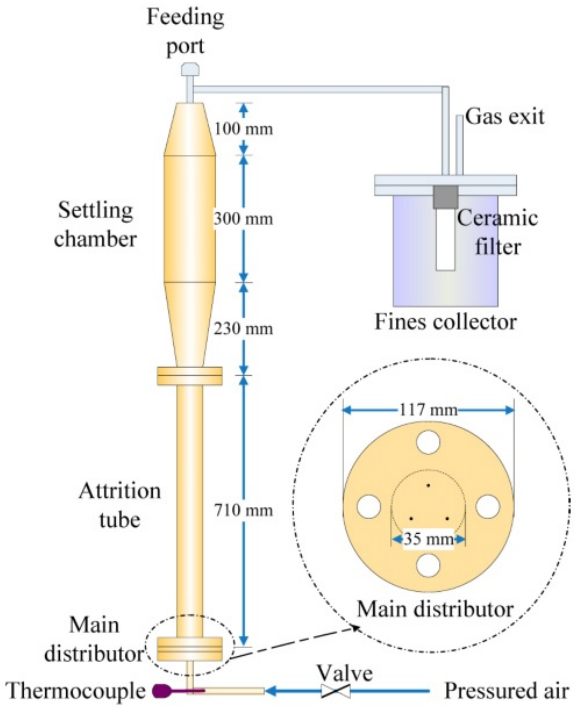

Figure 2.2 Air jet attrition testing apparatus [39]

.

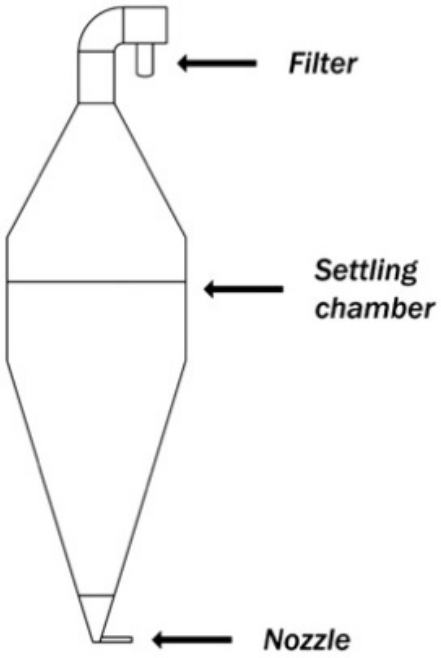

Figure 2.3 Jet cup set up [58]

.

2.5.2 Jet cup attrition testing

The Most common jet cup used is the Grace-Davidson model, which has a tangential gas inlet attached to a disengagement chamber (Fig. 2.3). A gas velocity of $150\,\mathrm{m\,s^{-1}}$ generates fines in the cup which are carried into the disengagement chamber. The process continues but fines escape through the outlet when they become small. This requires less powder sample as compared to cyclone attrition testing. An index of attrition representing an increase in weight fraction of fines less than $20\,\mu\mathrm{m}$ is calculated after an hour of test.

Ryden et al [58] measured the attrition resistance of two oxygen carriers meant for chemical looping combustion applications: NiO and Fe_2O_3 as active phase carriers with Al_2O_3 or $MgAl_2O_4$ as support. Freshly prepared oxygen carriers showed higher attrition resistance compared with those that have gone through cycles of chemical looping combustion with natural gas. Attrition resistance of the particles from the jet cup were also compared with their individual crushing strength. Cocco et al [43] increased the Davidson jet cup diameter to 7.6 cm and used it to compare the attrition resistance of equilibrium FCC catalyst and proprietary catalyst. Results from attrition studies with the conical jet cup were similar to results from a fluidised bed test. Attrition rates from the cylindrical jet cup were 10 % to 30 % lower compared with the conical jet cup. Zhao et al [59] evaluated the attrition resistance of slurry bubble column reactor (SBCR) catalysts with an ASTM based system. Fragmentation was the major cause of catalyst attrition. Attrition rates of SBCR catalyst in the jet cup and ASTM fluidised bed were similar [30]. Conditions in the jet-cup only simulate the degree a material's friability in cyclone and may not necessarily give the attrition rate at the distributor region in a fluidized bed reactor.

2.5.3 Fluidised bed attrition test

During fluidised bed operations, catalysts experience collisions with each other and with the walls of the reactor. This causes attrition due to abrasion and fragmentation which leads to elutriation of fines. The importance of this phenomenon has led to a number of investigations involving attrition behaviour of lime containing sorbents for CO_2 capture. Chen et al [63] investigated the attrition behaviour of synthetic sorbent supported with aluminate cement in a fluidized bed reactor. Optimal carbonation/calcination conditions were employed and the effect of parameters such as time, particle diameter and number of cycles and attrition rate based on median particle size (Eq. 2.10) were studied.

$$R_\mathrm{a} = -\frac{1}{D_{50,0}}\frac{dD_{50,N}}{dN} \tag{2.10}$$

where N is the number of cycles, $D_{50,0}$ and $D_{50,N}$ are the median particle diameters at initial and after N cycles respectively. The attrition rate was higher at high temperatures and during initial cycles. Equation 2.10 only measures attrition rate with respect to single particle and may not give a true reflection of attrition resistance of the material.

The attrition resistance of five limestones were investigated in a lab- scale circulating fluidized bed (CFB) reactor and pilot-scale CFB [36]. The attrition rate was calculated with (Eq. 2.11)

$$R_{\mathrm{a}} = -\frac{1}{M_{+75,t}} \frac{dM_{+75,0}}{dt} \tag{2.11}$$

where $M_{+75,t}$ and $M_{+75,0}$ represent mass of particles in the bed at time t and time zero; with size greater than 75 µm as beyond which attrition did not occur. Agglomeration due to wall effect occurred in the lab-scale CFBC reactor but calcination in the pilot-scale CFBC resulted in the sample losing 43 % of its weight. High velocities in a circulating fluidised bed can attrit particles greater than 75 µm. Similarly Gonzalez et al [64] investigated the attrition of two limestones at typical calcination/carbonation conditions in a CFB reactor. Attrition rate was higher during the first few cycles but it levelled off afterwards. Data was fitted with existing semi-empirical correlations to obtain the attrition rate constants.

The effect of time, gas velocity, temperature on limestone particle attrition was studied in a CFB reactor from 25 °C to 850 °C [65]. Attrition rate decreased at higher temperature probably due to changes in gas properties. An Arrhenius type of correlation was developed to describe the mean particle size. Broda et al [66] synthesized a calcium based sorbent stabilized by Al_2O_3 from the sol-gel technique and tested the attrition resistance of the sorbent in fluidised bed reactor. Results showed that attrition resistance of the material increased with increasing content of Al_2O_3. Charitos et al [20] performed an analysis of the attrition behaviour of calcium based sorbent using a 10 kWth dual fluidised bed reactor. The PSD of the raw $CaCO_3$ and CaO were determined at specific times. The rate of attrition was $2\,\%\,h^{-1}$. Attrition resistance (in terms of extent of attrition) of limestone and a synthetic sorbent supported with calcium aluminate cement have been measured at low and high temperature using a fluidised bed reactor. The synthetic sorbent had lower attrition rate compared with the natural limestone [67]. Pacciani [68] investigated the effect of CaO content on the attrition resistance of synthetic sorbent in a 30 mm diameter quartz reactor. The mass of elutriated fines was calculated from the difference in mass after the 20th cycle of carbonation and calcination. When the content of CaO was increased from 50 % to 75 %, the attrition rate increased 10 times. The criteria set by Vaux and Keairins have been applied in [69] to assess the attrition behavior of Ca-based sorbent by imparting four types of stress:

mechanical, kinetic, chemical and thermal, which are likely to be experience in fluidized bed operations. Cement seemed to have improved the attrition resistance in all stress cases.

Fennell et al [70] have tested the attrition resistance of Purbeck, Cadomin, Penrith, Glen Morrison and Havelock limestones in 30 cm reactor. Cadomin attrited more than any of the limestone with 9 % attrition rate in the first carbonation/calcination cycles but levelled off in subsequent cycles. A pilot scale dual fluidized bed system was used to test the attrition resistance of havelock limestone [71]. The reactor was made of calciner/regenerator in the circulating mode at 900 °C and and carbonator was fed with 15 % to 16 % CO_2. With feed in the range of 400 µm to 600 µm, fines of about 100 µm microns were captured in the cyclone and attrition was significant even up to the 25th calcination/carbonation cycle.

Bubble velocity cause intra particle collisions in fluidized beds. Various research groups have proposed several correlations for bubble induced attrition. Pis et al [72] found that the bubble attrition rate is independent of bed height (Eq. 2.12) but according to Xi [73], the rate is proportional to bed height (Eq. 2.13)

$$R_{\mathrm{a,bub}} = k_{\mathrm{bub}}(U_{\mathrm{g}} - U_{\mathrm{g,mf}}) \tag{2.12}$$

$$R_{\mathrm{a,bub}} = k_{\mathrm{bub}}(U_{\mathrm{g}} - U_{\mathrm{g,mf}})H \tag{2.13}$$

where the abrasion rate constant is (k_{bub}) and ($U_g - \mathrm{U_{g,mf}}$) is the excess gas velocity. Result from (Eq. 2.13) is more reliable as mass of elutriated fines depends on whether or not the height exceeds the transport disengagement height.

Fluid velocities in most laboratory fluidized bed attrition test are of the order of 1 m s^{-1} which may not able to induce any significant attrition. Moreover, perforated plate distributors which are preferred in industry cannot be used as they tend to induce jet attrition.

According to Thon et al[74], fluidized bed is the main source of catalyst attrition after simulating commercial conditions on the various vessels of in circulating fluidized bed.

2.5.4 Cyclone attrition test

The cyclone is an important part of circulating fluidised bed system. Operations such as removal of fine particles from gas stream in cyclones usually lead to catalyst attrition.

Thon and Werther [75] tested the attrition resistance of both used and fresh VPP and compared with FCC. The VPP was subjected to mechanical stress in gas cyclone. The

rate of attrition was higher for the fresh catalyst than the used VPP catalyst. The attrition propensity for VPO was also lower than that of the FCC. The mechanism of different catalysts attrition in cyclones was investigated by Reppenhagen and Werther [76]. They developed a model to relate the surface created by the attrition process to the spent kinetic energy. The attrition rate was found to be proportional to the surface mean diameter of the material. Catalyst attrit as they pass through cyclones in circulating fluidised bed. The solid loading, gas velocity and particle diameter are main factors influencing cyclone attrition. Abrasion dominated attrition can be calculated according to (Eq. 2.14) [29]

$$R_{\mathrm{a,c}} = K_c U_c^n U_{\mathrm{c,in}}^2 \tag{2.14}$$

where K_c is cyclone attrition rate constant, $U_{\mathrm{c,in}}$ is the solid-to-gas loading, n shows a power law dependence of attrition rate on the gas velocity, U_c.

Only few studies on cyclone attrition have been reported since a circulating fluidized bed must be installed. Other factors such as solids circulation and initial elutriable fines might contribute to the attrition rate in the cyclone.

2.5.5 Impact attrition testing

A test sample is entrained in gas flowing at a specific velocity to impact a target. The impact velocity is a combination of the gas velocity and the terminal velocity of the particle. Particles are collected and analysed after impact.

Scala et al [77] tested the impact damage propensity of lime stone. Attrition rate varied with impact velocity. Particle impact attrition was also carried out at 25 °C to 580 °C and velocities between $9\,\mathrm{m\,s^{-1}}$ to $64\,\mathrm{m\,s^{-1}}$. A model to predict particle evolution of particle size distribution taking mass transfer between numbers of size classes was developed. The temperature effect on attrition rate followed the Arrhenius dependency. Lower attrition rates occurred at higher temperatures [78]. Similarly Chen et al [79] performed impact attrition of limestone at 25 °C to 580 °C and $20\,\mathrm{m\,s^{-1}}$ to $100\,\mathrm{m\,s^{-1}}$ impact velocity. Attrition rate decreased with increasing temperature due to reduced impact velocity and the impact activation energy was $5.2\,\mathrm{kJ\,mol^{-1}}$. This test method however does not simulate attrition that takes place in fluidised reactors.

2.6 Factors affecting attrition resistance

Attrition resistance of a material depends on three factors; process (temperature, pressure, velocity, time) and material factors (particle size, shape, porosity) and system design (orifice and distributor design). The conditions that prevail during attrition test dictates the attrition propensity of the material. Increasing temperature of gas reduces momentum transferred to materials through the density of the gas, thus decreasing the attrition rate of the material. However, some studies have shown that attrition rate of certain materials such limestone increase with increasing temperature due to changes in material properties. Similarly, increasing the pressure of the gas increases the attrition rate since the volume of gas decreases at higher pressure. The attrition rate increases with test time in a non-linear fashion.

Cairati et al [60] investigated the effect of time on attrition rate and concluded that the 1h duration may be insufficient for catalyst to reach an equilibrium attrition rate as suggested by Forsythe and Hertwig [37]. Gas and particle velocities in a fluidised bed are, perhaps, the process variables with the greatest influence on materials attrition propensity. Both jet and bed velocity increase the attrition rate [29]. Particle size distribution on material determines the surface area exposed to abrasion and the energy-to-size ratio. Reduced particle size means decreased energy- to- surface area ratio and reduced attrition rate. Rounded surfaces are more difficult to break as they contain fewer imperfection that may have been abraded off. Larger particles are more susceptible to fragmentation because they possess greater entropy of information and hence higher chance that they will be involved in breakage causing collisions [29, 55] according to the Boltzmann's theory. Lin and Wei [61] found that increasing temperature and gas velocity and decreasing particle size increased attrition rate of particles. Due to increased thermal stress and internal pressure, rate of particle fragmentation and hence attrition increased when temperature was raised [62].

2.7 Fluidized beds

When a fluid is passed through a bed of particles at low flow rates and the bed retains its integrity, it is called fixed bed (Fig. 2.4) With increasing flow rates beyond minimum threshold the bed behave like a fluid. Many methods have been devised to monitor pressure drop through a bed of packed fine particle as the velocity is increased or decreased. The commonest one is the ASTM method D7743 [80]. Equation (2.15) relates pressure drop and gas velocity for uniformly sized particles such as sand.

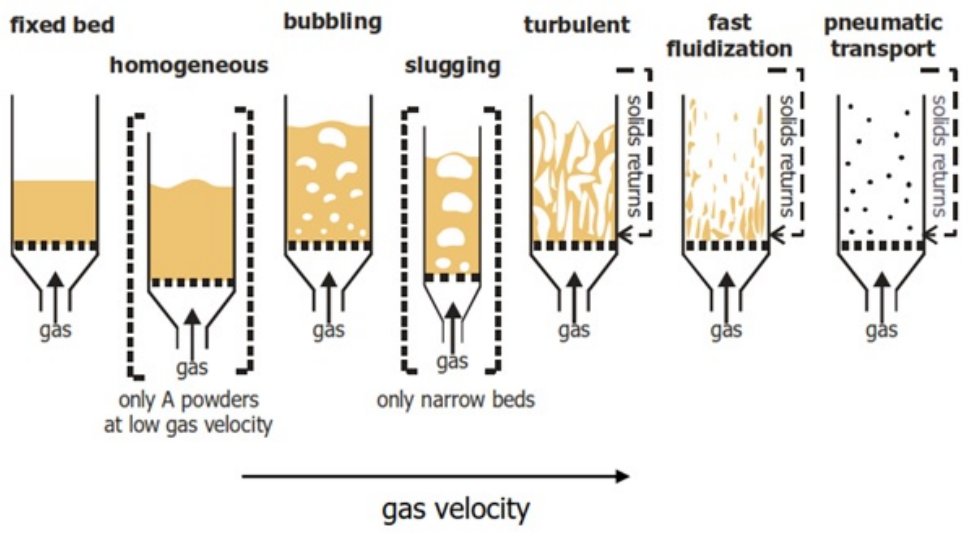

Figure 2.4 Fluidization regimes [81]

.

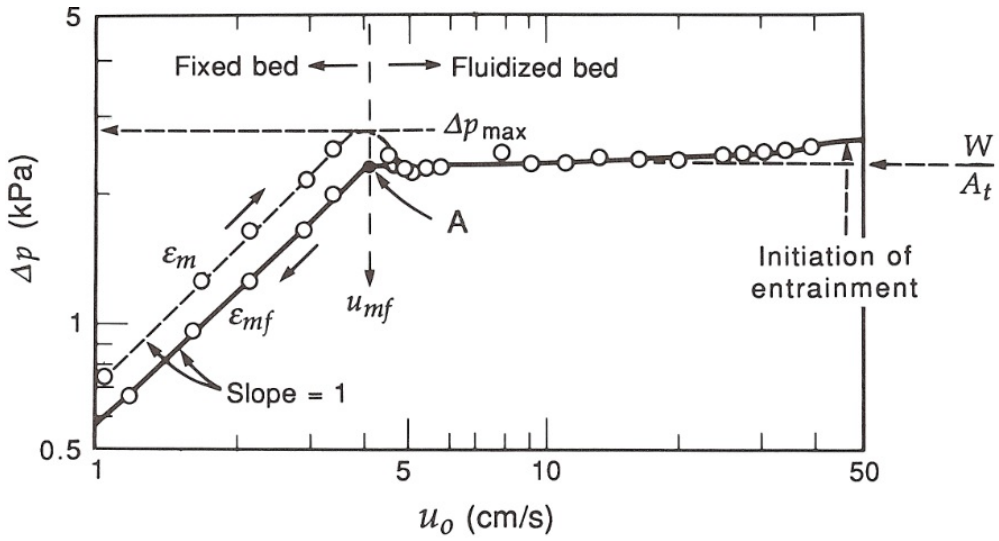

Figure 2.5 Pressure drop against fluidizing velocity for group B particles [81]

.

$$\frac{\Delta P g_c}{L} = \frac{150(1-\xi_{mf})^2}{\xi_{mf}^3}\frac{\mu U^{\,2}}{\phi d_p} + \frac{1.75(1-\xi_{mf})}{\xi_{mf}^3}\frac{\rho_g U^2}{\phi_s d_p} \tag{2.15}$$

$$Ar = \frac{150(1-\xi_{mf})Re_{p.mf}}{\phi\xi_{mf}^3} + \frac{1.75Re_{p.mf}^2}{\phi_s\xi_{mf}^2} \tag{2.16}$$

$$Ar = \frac{\rho_g(\rho_p-\rho_g)d_p^3}{\mu^2} \tag{2.17}$$

where ϕ_s, ξ_{mf}, $Re_{m,f}$, U, μ and Ar refers to particle sphericity, void fraction, Reynolds number at minimum fluidization, fluid velocity, gas viscosity and Archimedes number (Eq. 2.17), respectively. The first and second terms on the right hand side of (Eq. 2.15) are contributions made by viscous and kinetic energy losses respectively to the pressure drop per unit length of the bed. The former predominates at low Reynolds number and pressure drop across the bed has a linear relationship with gas velocity whereas the later predominates at high Reynolds number and the pressure drop increases as the square of the gas velocity. Depending on factors such as bed geometry, particle characteristics, bed voidage, when gas velocity is relatively low , the pressure drop of across the bed increases proportionately with increasing gas velocity (Fig. 2.5) This continues until the pressure drop is just above the static bed pressure.

As the gas velocity is increased further, a point is reached when the bed voidage increases and leads to reduced resistance to gas flow through the bed thus reducing the pressure drop back to the bed static pressure. This is the point when the bed just begins to behave like a fluid and the gas velocity is called minimum fluidization velocity. At this stage the drag force of gas equals the weight of the bed. The pressure drop across the bed ceases to increase even if the gas velocity is increased since the viscosity of the bed is relatively low. When the superficial velocity of the gas is increased beyond the minimum fluidizing velocity, bubbles appear near the distributor, increase in size to maximum, rise to the surface and erupt. The bed at this stage is called a bubbling bed. With further increases in gas velocity, the bubble size approaches the diameter of reactor vessel and top surface rises and breaks frequently. The bed at this stage is said to be slugging. With still further increases in gas velocity above the slugging velocity, turbulent regime is reached where the top surface of the bed is not clearly defined. Above the turbulent velocity, fast fluidization regime predominates where the top surface of the bed is non-existent; the bed is thrown out of the vessel and must be returned. The bed ceases to exist with further increase in the gas velocity. All particles are immediately entrained out of the bed and this stage is called pneumatic conveying [81].

2.7.1 Particle characteristics

Particles characteristics are usually described in terms of diameter, density, shape and morphology. The diameter of multiple particle systems is based on averages. The Sauter mean diameter is common in fluidization. It relates the external surface-area-to-volume of the particle. Since Sauter mean diameter describes the changes in surface area of particles, it is very useful in attrition process. Weight mean diameter describes changes in mass fraction of individual size class [82].

The shapes of particle are compared with that of perfect sphere. Sphericity of non spherical object introduced in [83] according to (Eq. 2.18).

$$\phi_p = \frac{\text{surface area of volume equivalent sphere}}{\text{surface area of particles}} \tag{2.18}$$

Based on particle shape, Chen et al [82] gave an empirical relation that suggests that the shape factor of particle evolves toward unity as the attrition proceeds. Ponomareva et al [86] showed that wear rate of fine particles changed when spherical lubricants were added to particles and that the wear rate increased with decreasing sphericity of lubricants.

The particle size distribution of typical fine particles is skewed towards the coarse region and the median particle size splits the distribution into two equal halves. This makes the median particle size the most appropriate to represent the central tendency of the distribution. Size distribution of solids particles resulting from size reduction can be assumed to follow a log-normal distribution. Xiao et al, [55] gave a log-normal model of the evolution of particle size in a jet mill attrition test and an quantified PSD of entrained fines with entropy of information function. The log-normal distribution corrects the normal distribution when it is skewed toward the positive direction.

2.7.2 Classification of powders

Geldart [86] gave a comprehensive grouping (A,B,C,and D) of powders for applications in fluidized bed processes (Fig. 2.6). This was based on fluidization data acquired at ambient conditions with air as the fluidizing medium.

The graph is plot of the density difference between the solids and air verses Sauter mean diameter of particles. Thus particles are located based on density difference and their mean size.

Group A powders can easily be fluidized but there is a difference between the velocity at which fluidization occurs and the first appearance of bubbles. Density of group A powders

is less than 1400 kg m^3 with size ranging from 30 µm to 100 µm.

Group B powders, which have densities between 1400 kg/m^3 to 4000 kg/m^3 and sauter mean diameter 100 µm to 1000 µm are easily fluidized but the minimum fluidizing velocity and minimum bubbling velocity are approximately the same. Group C powders with particle Sauter mean diameter between 0 µm to 30 µm are normally difficult to fluidize and results in frequent channelling due to stronger inter-particle forces. Group D powders are very large (size greater than 1000 µm) and are suitable for spouted bed applications. The Geldart classification is applicable at ambient temperature and with air as the fluidizing gas.

Both FCC and VPP catalysts belong to group A powders. The four sorbent compositions and cadomin used in this work are Geldart group B powders.

Grace [87] gave a new boundary between groups A and B at temperature and pressure above ambient and applicable to other gases. Goossen [89] classified powders based on Archimedes number equal to 88.5 (compared with Grace's Ar value of 125) as the boundary between groups A and B. Goossen's classification is valid even with liquid fluidized systems. Molerus [90] also reinterpreted Geldart's classification based on interparticle cohesive forces. Yang [91] modified Geldart's classification by plotting dimensionless density ration against Archimedes number. This allowed different powders to be compared at varying temperature and pressure.

2.7.3 Solids entrainment and elutriation

Gas velocity in fluidized beds may exceed the terminal velocity of particles and in jet induced flows, sonic and supersonic conditions occurs frequently. This situation results in entrainment and subsequent elutriation (selective removal of fines of particular size range) of attrition generated fines from the reactor vessels. Elutriation occurs either by direct removal of fines or the bursting bubbles [92]. It is important to keep track of elutriation in order to properly design dust collection systems such as cyclones and filters.

Solids entrainment occurs near the tip of nozzles. Fragmentation changes particle size distribution but it does not affect the elutriation rate significantly [93]. Elutriation is limited by both particle entrainment at bed surface and carrying capacity of fluidizing gas. Choi et al [94] studied the effect of fine particle on elutriation of coarse materials. The upward momentum of fines and gas velocity were proportional to the elutriation rate of coarse particles. Elutriation rate constant of Geldart A and C depend on relative humidity of the fluidizing gas, particle size [95] and weight fraction of fines of group C powder in the bed [100].

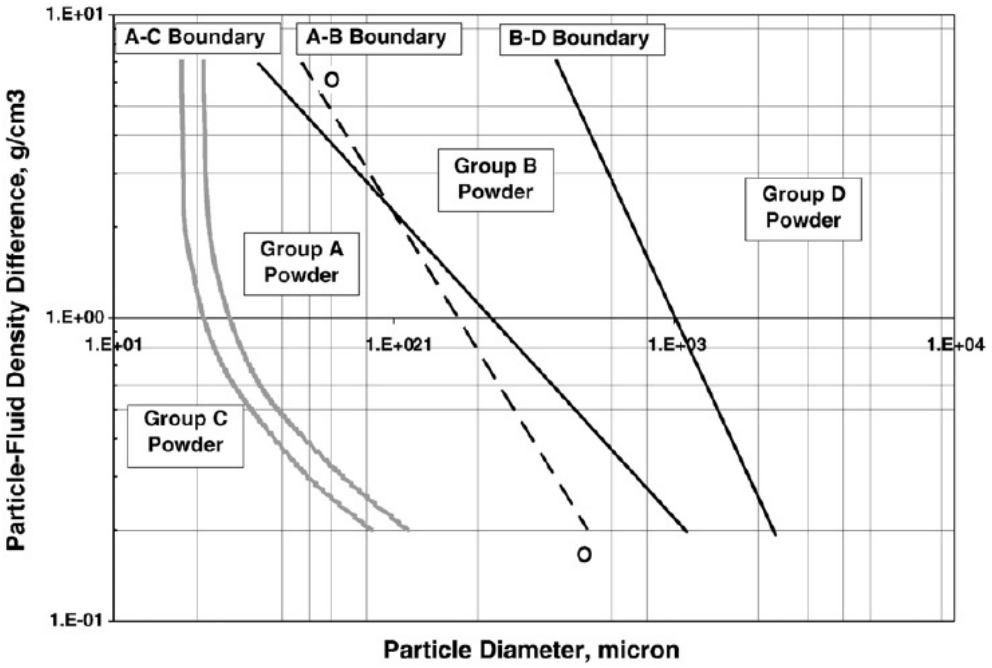

Figure 2.6 Geldart's classification of powders [86]

Correlation	Uo, m/s	Author
$\frac{L_i}{d_o} + 4.5 = 5.25\left(\frac{\rho_f d_o}{\rho_p d_p}\right)^{0.3}[1.3]\left(\frac{U_j^2}{d_o}\right)^{0.2} - 1$	40-200	Merry, 1971
$0.0144\frac{L_{max}}{d_o} + 1.3 = 0.5\log(\rho_f U_j^2)$	32-64	Zenz, 1968
$\frac{L_i}{d_o} = 814.2\left(\frac{\rho_f d_o}{\rho_p d_p}\right)^{-0.585}\left(\frac{\rho_f d_o U_j}{\mu}\right)^{-0.654}\left(\frac{U_j^2}{g d_o}\right)^{0.47}$		Wen et al , 1977
$\frac{L_i}{d_o} = 5.52\left(\frac{\rho_o U_j^2}{(\rho_p - \rho_f) g d_o}\right)^{0.27}$	15-300	Benjellou, 1991

Figure 2.7 Correlations for jet penetration length

.

2.7.4 Jet penetration

Formation of standing jets is characteristic of high velocity nozzles. The concept of jet penetration in fluidized is very important since the penetration length, jet momentum dissipation and jet half angle are critical design parameters. These parameters are important for intense gas –solid mixing and consequently good heat and mass transfer in fluidized bed reactors. Yang and Keairns [100] modelled jet penetration length with a two-phase Froude number (Eq. 2.19).

$$\frac{L_i}{d_o} = \frac{\rho_f U_j^2}{\rho_p - \rho_f} g d_o 0.5 = 6.5(Fr)^{0.5} \tag{2.19}$$

where ρ_{f}, ρ_{p}, U_j and Fr refers to fluid density, particle density, jet velocity and Froude number respectively.

This relation sparked several investigations into jet penetration and their various correlations as functions of process conditions such as orifice diameter and gas velocity (Fig. 2.7). In order to prevent erosion, bed internals such as baffles and heat exchangers tubes should not be placed in jetting region near the grid. Upwardly directed jet penetration can vary up to about 30 % [101] . The momentum dissipation of jet affects its penetration length (Fig.2.8) Yang [90] suggested (Eq. 2.20) to calculate momentum dissipation of the jet.

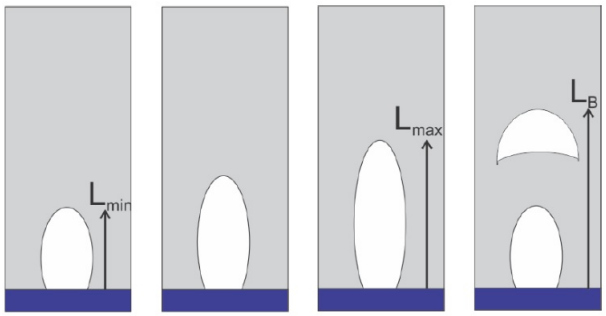

Figure 2.8 Jet penetration length.

$$\frac{U_i}{d_m} = \frac{0.26 x_i}{d_o} \tag{2.20}$$

2.7.5 Critical flow nozzles

Design of orifice plate (Fig. 2.9) in jet induced attrition follows the convergent-divergent nozzle design criteria as an isentropic process. The orifice plate consists of a rounded inlet

Figure 2.9 Flow nozzles

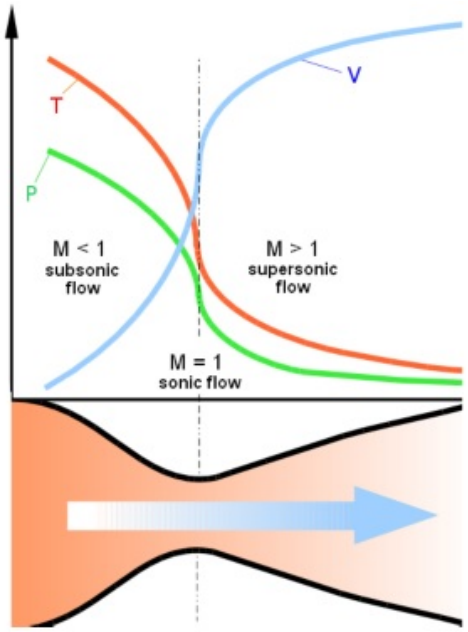

Figure 2.10 Mach number variation with flow properties [102].

which converges to a minimum throat and pressure recovery divergent section. Important design parameters in the convergent-divergent nozzles include stagnation ambient pressure ratio and exit to throat area ratio. Fluid flow is sonic at the throat when the Mach number is one but changes to subsonic in the divergent section. Fluid velocity does not change when critical pressure ratio (Eq. 2.21) is reached. Fig.2.10 shows how fluid temperature, pressure and velocity changes with the Mach number [102, 103]. Assuming an ideal behaviour, mass flux of a sonic flow is calculated with (Eq. 2.22).

$$\frac{p^*}{P_o} = \frac{2}{k+1}^{\frac{k}{k-1}} \tag{2.21}$$

$$G = C_d A_o \sqrt{(\frac{2}{k+1})^{\frac{k+1}{k-1}} \times \frac{kM}{RT_o}} \tag{2.22}$$

where k is specific heat ratio, p^* is downstream pressure, p_o is nozzle upstream pressure, M is molar mass C_d is discharge coefficient.

2.7.6 Grid design

The grid is very important and its design must be carefully done to ensure smooth fluidization, prevent plugging and powder weeping into the plenum. Pressure head of solids through a fluidized bed affects resistance to fluid flow through the bed. Pressure drop (ΔP_{grid}) across the grid is calculated with (Eq. 2.23) [101].

The velocity through the grid is given by

$$U_h = C_d \sqrt{\frac{2\Delta P_{\text{grid}}}{\rho_f}} \tag{2.23}$$

$$Q = N U_h \frac{\sqrt{\Delta} P}{\rho_f} \tag{2.24}$$

where N, U_h and d_h is the number of holes, gas velocity through the hole and hole diameter respectively.

The volumetric gas flow rate is given by

$$Q = N U_h \frac{\pi d_h^2}{4} \tag{2.25}$$

The pressure drop across a bed must always be greater than 25 cm of water and more than

30 % of pressure across the bed for an upwardly directed jet (Fig.2.8).

CHAPTER 3 ORGANIZATION OF THE THESIS

3.1 Original scientific hypothesis

1. Fluidized bed reactor provide an effective means of carrying out calcium looping and chemical looping combustion for post-combustion CO_2 due to high heat and mass transfer and minimization of hot spots.
2. High fluid velocities in fluidized beds cause high frequency sorbent particle-particle and sorbent particle-reactor wall collisions. These results in momentum transfer between particles leading to mechanical degredation (attrition) of sorbent particles, production of fine particles and subsequent elutriation of fines of particular cut size.
3. Mechanical properties of sorbents are critical to their economic and environmental effectiveness.
4. High temperature requirement in Calcium looping-chemical looping combustion causes sintering of sorbent and lead to reduction in reactivity performance of sorbent.

3.2 Methodology

The project consisted three main phases.

1. The first phase involved acquisition of the various sorbents compositions and the purchase and installation of industrial jet attrition testing device for low temperature operation. The setup was then adapted to high temperature testing with the acquisition of furnace capable of heating up to 1100 °C.
2. Preliminary studies was conducted to compare the attrition resistance of $CaO_{40}CuO_{50}Cement_{10}$ sorbent with those of two commercial catalyst: Dupont's VPP catalyst and FCC catalyst.
3. Detained studies including measurement of attrition resistance of different compostions of sorbent, FCC ans VPP at vagarious process and design conditions.

3.3 Article

To realise the above objectives, a paper entitled: Attrition resistance of $CaO_xCuO_ycem_{1-x-y}$ powder for CO_2 capture in calcium looping processes has been presented in chapter 4 (main

body of the thesis). It compares the mechanical stability of Ca-based CO_2 sorbents with two commercial catalysts: DuPont's VPP and FCC. The paper gives detailed analysis of the changes in the particles size distribution from 6 h to 96 h and 23 °C to 800 °C. A model was then developed to predict the attrition rate of the sorbents.

CHAPTER 4 ARTICLE 1: ATTRITION RESISTANCE OF CaOxCuOycem1-x-y POWDER FOR CO2 CAPTURE IN CALCIUM LOOPING PROCESSES

Peter Asiedu-Boateng, Robert Legros, Gregory S. Patience.
Department of Chemical Engineering,
Polytechnique Montréal, C.P. 6079, Succ. CV Montréal,
H3C 3A7 Québec, Canada.

(Submitted to Powder Technology, April 2015)

4.1 Abstract

Integrating calcium looping (CaL) and chemical looping combustion (CLC) is potentially more energy efficient than existing technology for post-combustion CO_2 capture. Mixtures of CaO, CuO and cement (cem) are promising sorbents but attrition losses due to abrasion and fragmentation could incur an unacceptable economic penalty. In jet mills, which test attrition resistance due to impact, $CaO_xCuO_ycem_{1\text{-}x\text{-}y}$ sorbents mechanical stability is comparable to crushed cadomin limestone, vanadyl pyrophosphate (VPP) and fluid catalytic cracking (FCC) catalyst. The attrition rates of VPP and FCC at an orifice gas velocity of $180\,\mathrm{m\,s^{-1}}$ were $5\,\mathrm{mg\,h^{-1}}$ and $7\,\mathrm{mg\,h^{-1}}$, respectively; it was $10\,\mathrm{mg\,h^{-1}}$ for $CaO_{40}CuO_{50}cem_{10}$. The attrition rate increases with the square of the orifice diameter, almost the fourth power of the gas velocity and to the power 0.4 with gas density. The attrition rate doubles at 800 °C for $CaO_{90}cem_{10}$ but is essentially constant for $CaO_{40}CuO_{50}cem_{10}$: the particle size increased with increasing temperature in the jet mill that is due to particles agglomerating. The fragmentation rate — mother particles ($d_p > +400\,\mu m$ breaking in to several daughter particles ($d_p < --400\,\mu m$ — of the $CaO_xCuO_ycem_{1\text{-}x\text{-}y}$ sorbents was an order of magnitude higher than the attrition rate.

4.2 Introduction

Two thirds of global anthropogenic carbon dioxide emissions are attributable to burning fossil fuels [1]. In 2012, fossil fuels contributed 82 % of the global energy demand and it is predicted to increase 37 % by 2040. Since 1958, the CO_2 concentration has increased by almost 100 ppm [104]. It has risen exponentially and will reach 450 ppm (Eq. 4.1) by 2040 if it continues on the same trend (Figure. 4.1).

$$CO_2 = 317 + 0.28\,(y - 1958)^{1.4} \tag{4.1}$$

It is imperative to mitigate the impact of CO_2 emission might have on the environment. Substituting fossil fuels with renewable sources - wind, solar, geothermal and hydro are the preferred option but the economics remain uncompetitive in many applications - particularly for automotive and power.

Carbon capture and sequestration (CCS) adds to the cost and CO_2 emissions from fossil power generation plants. Three steps make up CCS: CO_2 capture (15 \$/t to 75 \$/t), transport (1 \$/t to 8 \$/t) and storage (0.5 \$/t to 8 \$/t) [105]. The broad ranges for the cost of each step relate to the technology options. Currently, amine scrubbing, contacting CO_2 rich flue gas with aqueous monothanolamine (MEA) flowing counter-currently is the only technology practised commercially. MEAs scrubbing is inefficient [5, 6, 106].

Dry solid sorbent technologies are gaining prominence as an alternative to aqueous solvents to capture CO_2. The calcium oxide-calcium carbonate couple has superior economics and energy efficiency [8, 9, 10]. In this process calcium oxide scavenges CO_2 from the flue gas and forms calcium carbonate. Oxygen reacts with the $CaCO_3$ to give CaO in a second vessel which returns it to the flue gas stream. Separating oxygen from air introduces an economic penalty with respect to investment and operating cost.

Integrating calcium looping (CaL) with chemical looping combustion (CLC) eliminates the need for an air separation unit. In this technology, a metal oxide supplies the oxygen to convert $CaCO_3$ to give CaO rather than pure oxygen. Canmet Energy is developing a CaO-CuO sorbents with a calcium aluminate cement binder [12, 23]. Besides reactivity and stability, another consideration to commercialize this technology is minimizing attrition that arises due to abrasion (particle-wall contact in cyclones,for example) and particle-particle and particle wall collisions (particularly at high velocity nozzles). Evaluating the mechanical properties of the novel sorbent is the first undertaking to assess its suitability together with oxidation —regeneration cycles. Attrition can render the capture process economically unattractive. Moreover, it can be a serious health and environmental problem with sorbents containing toxic metals such as Ni.

4.3 Theory

The attrition rate (R_a) is the fractional loss in solids mass (M) with time (t).

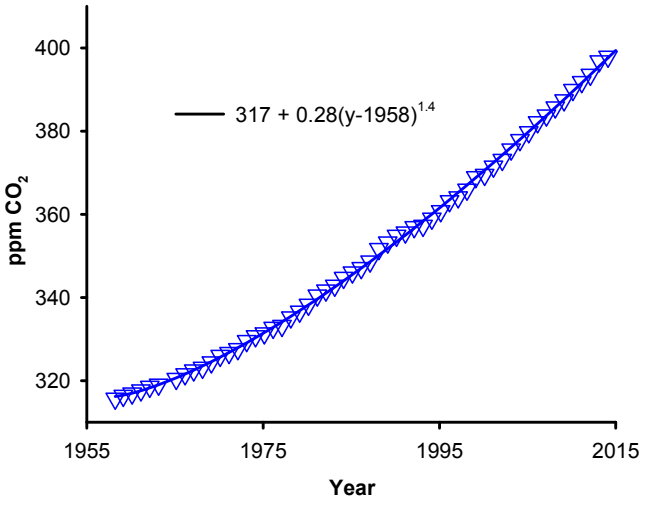

Figure 4.1 Historical atmospheric CO_2 concentration (ppm) reported by the Mauna Loa observatory [104].

$$R_{\mathrm{aj}} = \frac{dM}{dt} \tag{4.2}$$

Forsythe and Hertwig [37] measured impact attrition rates in air jet mills. Gwyn [33] improved on this work that later gave rise to the ASTM D5757 standard and proposed the following exponential relationship

$$R_{\mathrm{aj}} = kt^m \tag{4.3}$$

where the index m varies between 0.43 - 0.9. Subsequently, other tests have been developed including the jet cup [43, 59], cyclonic [29, 56], particle impact [77, 78, 79] and fluidised beds [36, 63, 64].

Werther and Xi [56] related jet induced attrition rate and the surface energy created with the energy spent (Eq. 4.4). They tested three fluidized geometries with fluid cracking catalyst catalyst. The supposed linear relationship between the attrition rate and input kinetic energy had a limited application range with respect to particle size.

$$R_{\mathrm{aj}} = k_j n_{\mathrm{o}} \rho_{\mathrm{g}} d_{\mathrm{p}} d_{\mathrm{o}}^2 U_{\mathrm{o}}^3 = k_j d_{\mathrm{p}} \dot{m} U_{\mathrm{o}}^3 \tag{4.4}$$

where k_j is material specific attrition constant, ρ_{o} is gas density, d_{o} is orifice diameter, U_{o} is orifice gas velocity and n_{o} is the number of orifices. Thon et al [74] express the attrition of

each particle fraction(Eq. 4.5)

$$R_{\mathrm{aj,i}} = k_j d_{\mathrm{p,i}} \dot{m} U_{\mathrm{o}}^2 \Delta Q_{2,\mathrm{i}} \tag{4.5}$$

where $\Delta Q_{2,\mathrm{i}}$ represents the fraction of surface area of the particles in an interval, i. Ghadiri et al [57] proposed a general relation for fluid cracking catalyst attrition rates based on a single particle impact test that represents the jetting region of fluidised bed (Eq. 4.6).

$$R_{\mathrm{aj}} \propto u_o^{(m+2.34n)} \tag{4.6}$$

where m and n depend on orifice conditions(Eq. 4.6). The exponent on the orifice velocity (3.31) was predicted at an orifice diameter of 2 mm and velocity from $8\,\mathrm{m\,s^{-1}}$ to $25\,\mathrm{m\,s^{-1}}$. The model, however, did not clearly indicate which criterion (jet height or maximum particle velocity) determines the value of the exponent.

Thon and Werther [75] evaluated the attrition rates of both equilibrated and calcined VPP catalyst in cyclone and fluidised beds with submerged gas jets. The equilibrated catalyst Attrition resistance of equilibrated VPP catalyst was higher than that of calcined VPP catalyst in the cyclone. However, the attrition rate of equilibrated VPP was higher in the fluidised bed compared to the calcined VPP. Abrasion was the main mechanism of attrition. Conditions prevailing in cyclones will not apply to small jet mills.

McMillan et al [107] measured coke and sand attrition rates due to gas injected through sonic nozzles into fluidized beds. They report that the particle breakage frequency (attrition rate) was independent of the mass of solids in the bed and that it depended mostly on the nozzle geometry, operating conditions and fluidized bed velocity.

$$R_{\mathrm{aj,i}} = k_j \alpha \beta d_{\mathrm{N}}^{1.131} U_{\mathrm{N}}^{0.55} \left(\rho_{\mathrm{g}} U_{\mathrm{N}}^2\right)^{1.635} \left(\frac{U_{\mathrm{g}} - U_{\mathrm{mf}}}{U_{\mathrm{mf}}}\right)^{0.494} \tag{4.7}$$

where α is an index related to type of solid ($\alpha = 1$ for silica and $\alpha = 0.8$ for coke), β is a geometry coefficient and the index, N, relates to nozzle diameter (Eq. 4.7). This relationship applies to nozzles immersed in fluidized beds rather than orifices in small units.

A jet mill measured the VPP attrition resistance catalyst during the development of DuPont's CFB process [48]. In the pre-pilot stage, a 1.4 m Bowen spray dryer produced the porous micro-spheres. After the powder was calcined in air, its attrition resistance was $18\,\mathrm{mg\,h^{-1}}$ at an orifice velocity of $232\,\mathrm{m\,s^{-1}}$ and a 0.4 mm orifice. A 2.8 m spray dryer produced VPP for the pilot plant. The calcined micro-spheres from the larger spray dryer were twice as resistant. Finally, an 8 m spray dryer produced the VPP for the commercial plant and its

mechanical resistance improved to $4\,\mathrm{mg\,h^{-1}}$ [49].

Typically, catalytic fluidized bed reactors operate with Geldart Group A powders with a d_{50} of 70 µm. Sorbents and metal oxides in CaL and CFB process are as much as an order of magnitude larger. The reactors operating temperatures' can exceed 800 °C and so non-mechanical valves and Geldart Group B powders control solids circulation rates.

The high temperatures and larger particles may result in alternate attrition modes versus the catalytic processes. Lime particles from 710 µm to 850 µm particles mainly abraded but the same particles below 180 µm fragmented [55]. Enhancing the mechanical resistance is necessary to commercialize sorbents for CaL reactors [66]. With the ASTM D5757, Knight et al [40] tested many sorbent compositions produced by Canmet Energy and the University of Laval. The mechanical resistance of the calcium aluminate cement bound sorbent was better than the crushed limestone but it was inferior to the silica coated sorbent. The attrition rates at 500 °C were two to three times higher than the experiments at ambient conditions. They mention the competing mechanisms related to attrition due to temperature in that the gas viscosity increases with temperature but gas density decreases with temperature, so these two affects are confounded — assigning the cause for the higher attrition requires tests with different gases with either the same viscosity or the same density (to match the mass flow rate).

How well do atmospheric attrition tests predict attrition rates in commercial fluidized beds with nozzles that operate at lower gas velocities? It is unclear why the exponents on the factors for the jet attrition mill correlation (Eq. 4.5) are so different than for the nozzle immersed in a fluidized bed (Eq. 4.7). In the attrition mill, $R_{\mathrm{aj,i}}$ is proportional to the orifice diameter squared whereas it is linear for the nozzle; it is third order with respect to gas velocity for the orifice and almost 4th order for the nozzle; finally, it increases linearly with gas density in the orifice and to the power 1.6 in the nozzle. Besides, the work of [40] few data are published on the effect of elevated temperature (i.e. 500 °C) and even fewer at the operating temperatures of Calcium Looping and Chemical Looping combustion.

Here, we compare attrition resistance of commercial fluidized bed powders with four CaL-CFB Ca-based -aluminate cement bonded sorbents produced at Canmet Energy up to 800 °C, with three nozzle diameters with He, CO_2 and air and at gas velocities from $180\,\mathrm{m\,s^{-1}}$ to $230\,\mathrm{m\,s^{-1}}$.

4.4 Experimental methodology

4.4.1 Sorbents and catalysts

Canmet Energy combined a lime-based sorbent, CuO, and calcium aluminate cement as a binder ($CaO_{40}Cu_{50}cem_{10}$) — Table 4.1). The idea is to develop cost effective sorbent that integrates calcium looping and chemical looping combustion for post-combustion CO_2 capture. Crushed cadomin limestone from Alberta, Canada, served as the source of CaO (the active component) while CuO is the oxygen carrier. The binder particles, of which 80 % were below 45 µm, contain 71 % Al_2O_3 and 28 % CaO, The binder improves the mechanical stability, minimizes cost and reduces sintering [108]. A mechanical pelletizer produced sorbents after mixing the various components in the relative amounts. A solution of the compounds were spray dried to produce spheres, whose diameter were, in part, controlled by the quantity of $Ca(OH)_2$. Canmet Energy prepared other sorbents with varying amounts of binder — $CaO_{92.5}cem_{7.5}$, $CaO_{95}cem_5$ — to identify the effect of cement concentration on attrition resistance.

We compared the attrition resistance of these sorbents with DuPont's equilibrated VPP (catalyst has circulated in the plant at 400 °C for several years and presumed to have reached steady state attrition rate and hence termed termed equilibrated) and Y-zeolite fresh fluid catalytic cracking (FCC) catalyst. Steady state attrition rate means mass of fines generation does not change with time. The FCC catalyst contains macro-porous activated clay, mesoporous silica-alumina and zeolite. The activated clay also act as binder and improves its attrition resistance.

Canmet Energy sieved the powder with a 60 mesh sieve (250 µm). This powder retained many finer particles so we re-sieved it again with a 60 mesh sieve (15 min on a Ro-tap Model E Sieve Shaker). We tested VPP with with a d_p of 80 µm to 120 µm). The size range of the FCC was from 80 µm to 180 µm).

Table 4.1 Sorbents and catalyst particle size and bulk density

Material	d_{50} µm	ρ_b kg m^{-3}
$CaO_{40}CuO_{50}cem_{10}$	500	1200
$CaO_{90}cem_{10}$	360	1100
Cadomin	390	1200
Equilibrated VPP	95	1120
Fresh FCC	120	870

4.4.2 Attrition mill

The attrition mill consists of a 25.4 mm cup in which we place an interchangeable metal plate with a single orifice (Fig. 4.2). The metal plate was was 6.4 mm thick and the orifice extended from the bottom to the "shroud" by 3.0 mm. We tested (0.39 mm, 0.45 mm and 0.5 mm) diameter orifices. The jet cup was made of 316SS that was 1.59 mm in diameter.

The length of the cup above of the orifice plate was 12 cm. It was positioned entirely in a three-zone electrical furnace (2640 W, 110 V) capable of reaching 1100 °C.

The metal cup was connected to a 915 mm quartz tube 25.4 mm in diameter. The quartz tube expanded to a diameter of 76 mm and the distance between the straight section and the exit was 760 mm. The gas exits the mill from the top and passes through a Erlenmeyer flask and a 0.3 µm thimble filter retains the particles.

In standard tests, we charged 20 g of powder to the jet cup. We tested gas velocities from 180 $\mathrm{m\,s^{-1}}$ to 230 $\mathrm{m\,s^{-1}}$ at 23 °C, 500 °C and 800 °C. We preheated air and measured the temperature before and after the orifice to achieve the desired temperature. All tests ran for at least 24 h. The attrition rate, $R_{\mathrm{a,j}}$ refers to the mass of solids the thimble filter collects from 6 h to 24 h, which was a DuPont convention. For the 4 day extended tests, we charged 40 g of powder to the jet cup and measured the weight of the solids in the filter once a day.

4.4.3 Sorbent and catalyst properties

An LA 950 Horiba laser diffractometer measured the particle size distribution of samples before and after each attrition test. A Scott meter measured bulk density (Table 4.1). A JSM-7600TFE field emission SEM recorded images of the solids. An automated Quantachrome instrument (Autosorb-01) determined the BET surface area and pore volume at −196 °C after degassing with nitrogen at 150 °C for 4 h.

The particles were irregularly shaped with a rough surface except the equilibrated VPP, which was almost perfectly spherical with no asperities. The particle surfaces were noticeably smoother after the high temperature tests (Fig. 4.3) which suggests that abrasion is a dominant mechanism. The smoothing was less evident after tests at ambient temperature.

The VPP, however, showed no noticeable surface changes at ambient temperature but at 500 °C VPP fragmented.

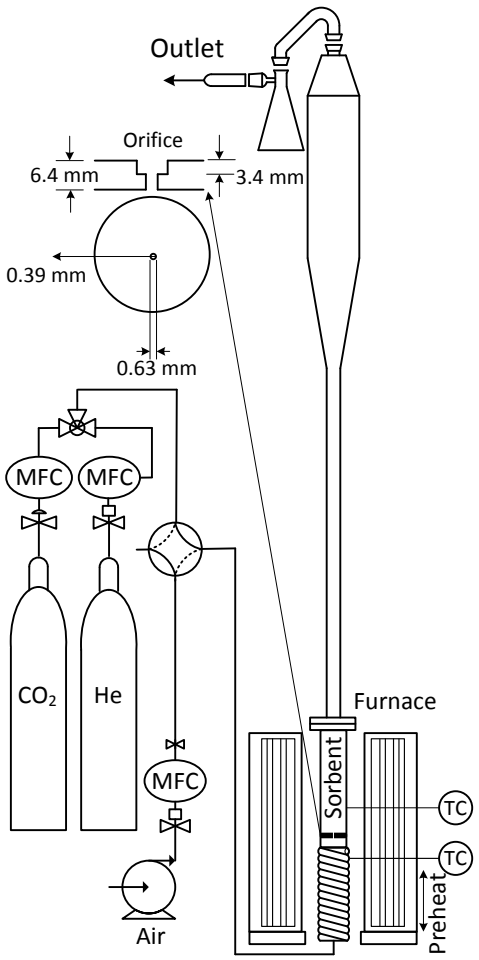

Figure 4.2 Jet attrition mill with a gas manifold for air, CO_2, and He. The electric furnace is rated for 1000 °C. The mill is made of stainless steal that is flanged to a quartz tube 25.4 mm in diameter.

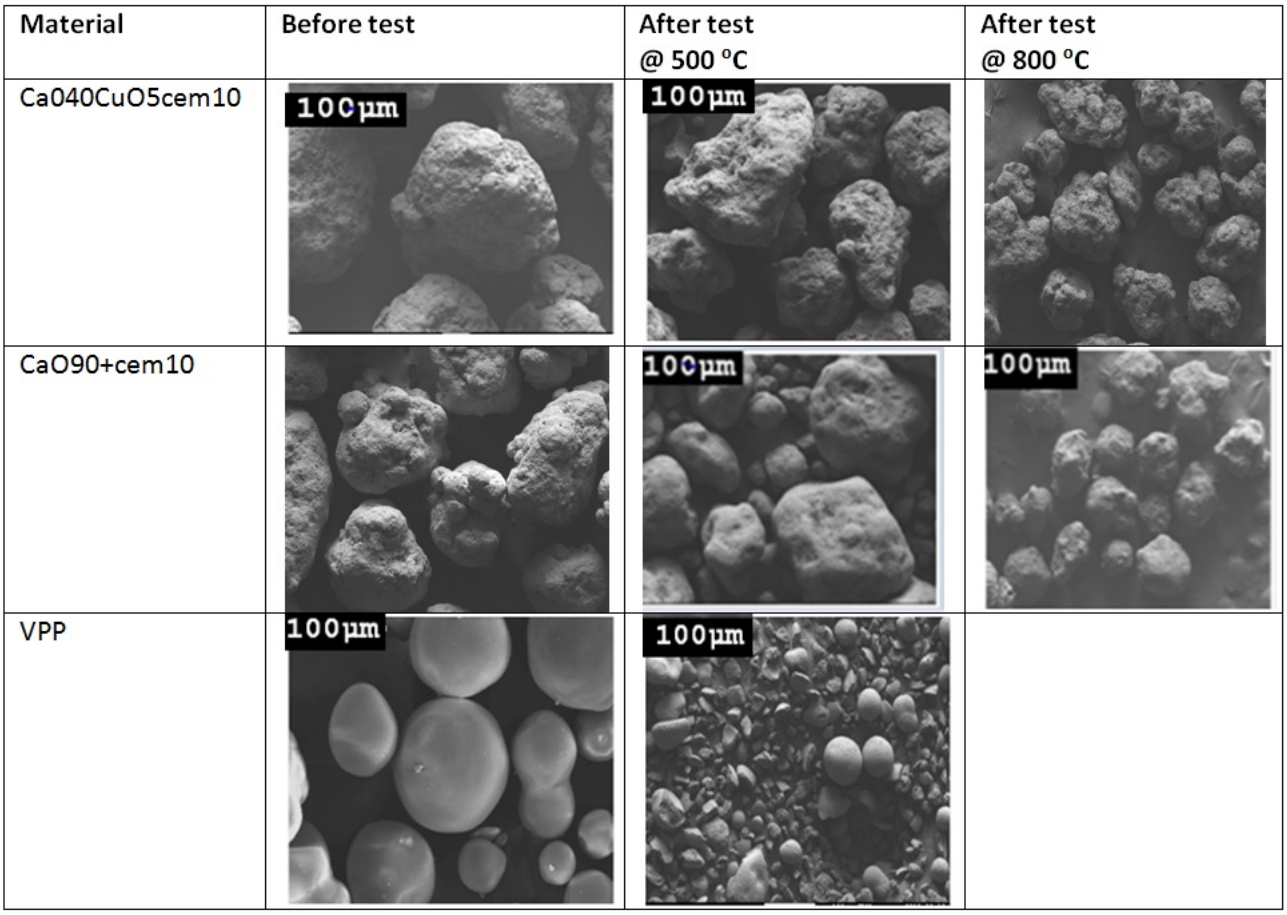

Figure 4.3 SEM images show that after 24 h and at 800 °C, the sorbents are noticeably rounder. Suprisingly, the VPP particles fell apart at 500 °C.

4.5 Results

4.5.1 Sorbent and catalyst attrition

We rank the mechanical stability of sorbents and catalysts based on the mass of fines trapped by the thimble filter between 6 h to 24 h under standard operating conditions: 0.39 mm orifice at 230 m s^{-1} and ambient temperature. The attrition rate of the equilibrated VPP was the lowest (13 mg s^{-1}) and the highest was the cadomin (32 mg s^{-1}) (Table 4.2). The mechanical stability of the $CaO_{90}cem_{10}$ was equivalent to FCC at (21 mg s^{-1}). It was 28 mg s^{-1} with 7.5 % cement and $R_{a,j}$ for $CaO_{90}cem_5$ was marginally lower at 29 mg s^{-1}.

Carbonated particles generally have a higher attrition resistance relative to the corresponding calcined particles [40, 67]. Since the sorbent undergoes carbonation-calcination cycles continuously it is important to assess the mechanical properties of both forms. During calcination, the sorbent releases CO_2 increasing the internal pressure, which may crack the particle (thermal decrepitation) [67]. To test the tendency to form cracks, we calcined the sorbent at 850 °C for 2 h. The attrition rate of the calcined sorbent almost doubled for all compositions except $CaO_{90}cem_{10}$, which increased by 50 % (Fig. 4.4).

Higher concentrations of cement improves attrition resistance. The uncalcined sorbent with 10 % cement was equally attrition resistant as the FCC. The attrition rates of the samples with 5 % and 7.5 % cement were 8 mg h^{-1} higher. Attrition rates of all the calcined sorbents are unacceptably high and require more cement.

Knight et al [40] identified three attrition modes — rounding of mother particles through abrasion (that elutriate from the jet cup); abrasion of fragmented particles (that elutriate from the cup); and, fragmentation, which may or may not elutriate depending on the particle size. An additional attrition mode is "shattering" where the particle breaks apart into micron

Table 4.2 Under the attrition mill's standard operating conditions the equilibrated VPP had the highest attrition resistance. Cadomin had the highest attrition rate. The d_{50} of all the powders dropped after 24 h in the attrition mill.

Powder	$R_{a,j}$	d_{50}, µm		
	mg h^{-1}	Before	After	Thimble
$CaO_{40}CuO_{50}cem_{10}$	26	490	390	4.3
$CaO_{90}cem_{10}$	21	450	350	2.9
Cadomin	32	380	230	2.1
VPP	13	114	94	7.0
FCC	20	130	118	3.8

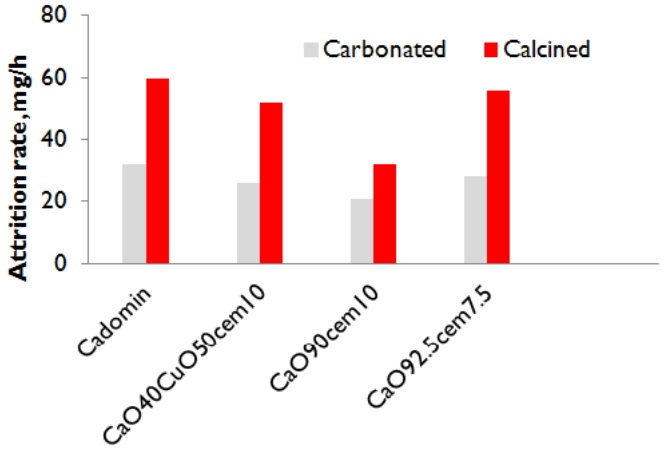

Figure 4.4 Effect of calcination on attrition rate. Calcining sorbents and VPP decreases mechanical stability.

sized powder and larger fragment that elutriate. When the binder is distributed throughout the particle, the main attrition modes are abrasion and fragmentation. When the binder is concentrated at the outer surface, like for a core-shell structure, the particles can shatter.

The jet mill test is incapable of quantifying each of these mechanisms if you only consider the solids that accumulate in the thimble filter (standard procedure). Fines in the thimble filter represent abrasion and rounding of asperities and shattering (where a sister particle is formed together with tiny pieces). Measuring the change in the PSD of the powder remaining in the jet cup assesses fragmentation. The PSD and SEM images can help substantiate the importance of each mode of attrition.

Eq. 4.4 characterizes the loss of fines to the thimble filter predominately due to rounding (cleaving) and shattering. The mill is designed such that most particles below 15 µm elutriate, which is close to the design criterion for commercial fluidized bed cyclones.

The d_{50} of the $CaO_{40}CuO_{50}cem_{10}$ was larger than the other four powders at 500 µm (Table 4.2). To assess the affect of time on attrition rate, we loaded 40 g of powder to the jet cup and ran it continuously for 96 h at standard conditions. During the first 6 h, fines elutriated at 40 mg h^{-1}. The rate remained constant thereafter at 23 mg h^{-1} (Fig. 4.5).

The fraction of particles below 200 µm before the attrition test was 1.5 % and this fraction increased to 9 % after 24 h in the attrition mill. After 96 h it rose to 30 %. The change in the fraction of large particles was the opposite: particles above 680 µm dropped from 11 % to 5.5 % after 24 h and then to 2.5 % at 96 h (Fig. 4.6).

During the entire test, mother particles fragment. They fragment faster in the first 24 h and

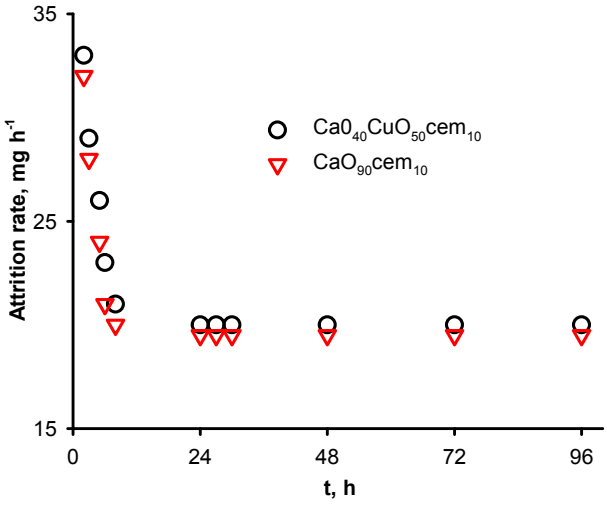

Figure 4.5 The attrition rate is constant after 6 h for both$CaO_{10}CuO_{10}cem_{10}$ and $CaO_{90}cem_{10}$.

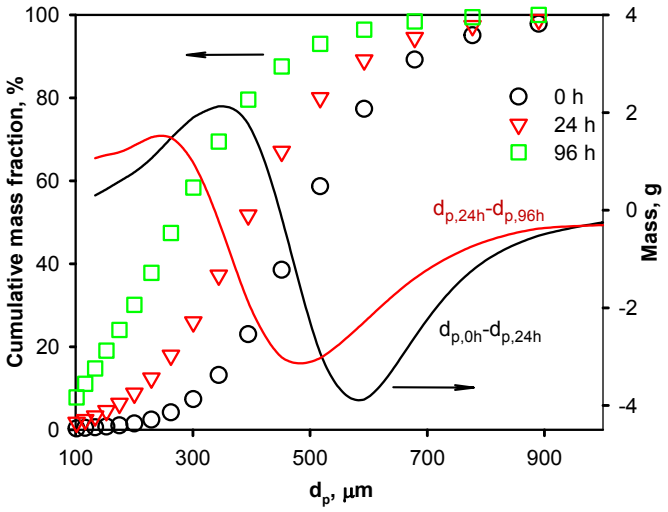

Figure 4.6 Symbols represent the PSD of uncalcined $CaO_{40}CuO_{50}cem_{10}$. The lines represent the difference in mass of solids for each particle size: black solid line is between 24 h and the virgin sample; the dashed red line between 96 h and 24 h.

then the rate drops during the following 72 h. The fines fraction is invariant with time with respect to the PSD and $R_{a,j}$ (Fig. 4.7). In the first 6 h, the thimble filter trapped 500 mg and at the end it collected 1900 mg.

The attrition rate trend was identical for $CaO_{90}cem_{10}$ as for the $CaO_{40}CuO_{50}cem_{10}$: the initial rate dropped from above 30 mg h^{-1} to a steady value of 20 mg h^{-1}. The PSD of the fines in the thimble filter after 6 h were identical to those after 24 h, which further suggests that the attrition mode is invariant with time, contrary to Gwyn's model (Eq. 4.3) that assigned a value of 0.4 or greater to the exponent on time.

A constant attrition rate indicates that the daughter fragments are equally attrition resistant as the mother particles. To substantiate this finding, a Tyler series sieve separated the sorbent into a 155 µm to 355 µm fraction and a fraction from 355 µm to 600 µm. The attrition rate of the smaller fraction was double that of the larger fraction: 52 mg h^{-1} versus 26 mg h^{-1}. This result agrees with earlier reports [40] but contradicts the attrition rate that is invariant with time. If smaller particles are more friable than larger particles, than the attrition rate should increase with time as the mother particles break up into daughter particles. The fraction of the daughter particles increase and therefore the attrition resistance should also increase. To account for this apparent contradiction, the daughter particles formed from fragmenting mother particles must be more mechanically resistant than the original *mother* particles of the same diameter. In other words, large mother particles are more attrition resistant than smaller mother particles and daughter particles formed from the larger particles are also more attrition resistant. (Remember that we define the attrition rate as the fraction of particles the thimble collects. We exclude fragmentation of larger particles).

More than 99 % of the elutriated fines in the thimble filter were less than 15 µm. The d_{50} of the $CaO_{90}cem_{10}$ fines was 2.9 µm, which is less coarse than the $CaO_{40}CuO_{50}cem_{10}$ fines (Table 4.2).

Mother particles fragmented most during the first 24 h — 12 g of the +400 µm formed particles in the range of 200 µm to 400 µm (Fig. 4.8). The fragmentation rate of the +400 µm dropped an order of magnitude from 670 mg h^{-1} (first day) to 44 mg h^{-1} during the following three days. The +250 µm –400 µm fraction increased by the same rate. During the last three days, mass of –250 µm was decreasing. The rate of change of these small particles ended up in the thimble filter ($R_{a,j} = 21$ mg h^{-1}).

The cadomin elutriated fines' shape was irregular (Fig. 4.9) and the average PSD was much smaller than all of the other fines at 2.1 µm. Both the carbonated form and the calcined form had the highest attrition rate. The d_{50} dropped from 380 µm to 230 µm (Table 4.2). More than 15 % of the powder left in the jet cup after the attrition test was under 50 µm and half

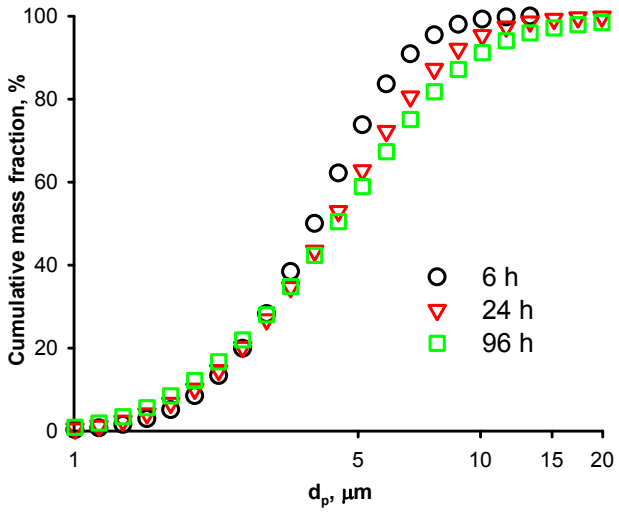

Figure 4.7 The PSD of fines are similar after 6 h, 24 h and 96 h in the attrition mill.

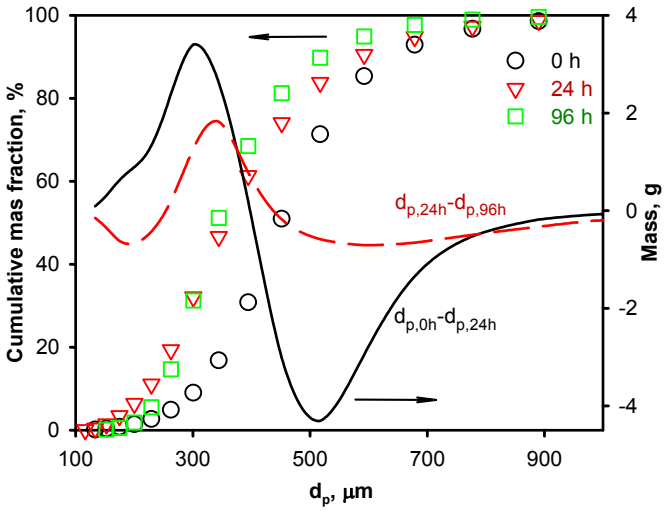

Figure 4.8 Mass of $CaO_{90}cem_{10}$ in each size increment before and after the attrition test and the difference between the two curves.

of these were below 20 µm. Surprisingly, the mill was incapable of elutriating these fines. The d_{sv} of the cadomin before the attrition test was 84 µm and it was 67 µm after the test. The large difference between the d_{50} and the d_{sv} is due to the fines fraction. The difference between the d_{50} and the d_{sv} of the $CaO_{40}Cu_{50}cem_{10}$ and $CaO_{90}cem_{10}$ was on the order of 50 µm.

Operating temperatures in commercial FCC risers exceed 600 °C. The dominant attrition mode is cleaving µm sized asperities (abrasion). The PSD of the fines fraction from the thimble filter confirm that abrasion dominates with the largest fraction of particles below 1 µm (Fig. 3.11). The average particle diameter dropped from 130 µm to just below 120 µm, which substantiates the fragmentation attrition mode.

The VPP powder is susceptible to shattering in which the hard silica shell cracks and spills the micro-sized powder in the interior. Prior to spray-drying the precursor, the vanadyl hemi-hydrate is micronized to 2 µm. In the spray drying process, the silica binder migrates to the surface and forms a resistant shell. The PSD from the fines in the thimble are greater than 5 µm, which indicates that the elutriated powder consists of an assemble of particles.

4.5.2 Effect of temperature

Calcium looping and chemical looping combustion operates in the range of 600 °C to 1100 °C, which may accentuate sintering, agglomeration and attrition. Sintering reduces the catalyst surface area and will also reduce its catalytic activity. Copper is particularly problematic for this application because it melts at the reaction temperature. A malleable catalyst might cover CaO active sites, it may also affect the mechanical integrity of the powder.

We tested $CaO_{40}CuO_{50}cem_{10}$, $CaO_{90}cem_{10}$ sorbents and VPP at ambient temperature, 500 °C and 800 °C while maintaining the jet velocity at 230 m s^{-1}. The attrition rate of $CaO_{90}cem_{10}$ increased by 50 % at 500 °C and more than doubled at 800 °C (Table 4.3). The +400 µm fraction attrited (Fig. 3.12). The mass of powder above this diameter decreased by over 5 g (out of the total of 20 g that we charged to the jet cup). The particle size decreased with increasing temperature while the surface area increased. The results of the $CaO_{40}CuO_{50}cem_{10}$ were the opposite. The particle size increased while the attrition resistance improved and the surface area was essentially constant. The powder agglomerates, presumably because of the copper but since the pore volume remained the same, sintering must be negligible (Fig. 3.14).

At low temperature, the VPP attrition rate was 13 mg h^{-1} but at 500 °C it shattered and the attrition rate trebled to 54 mg h^{-1}. This high attrition rate was unexpected since the catalyst

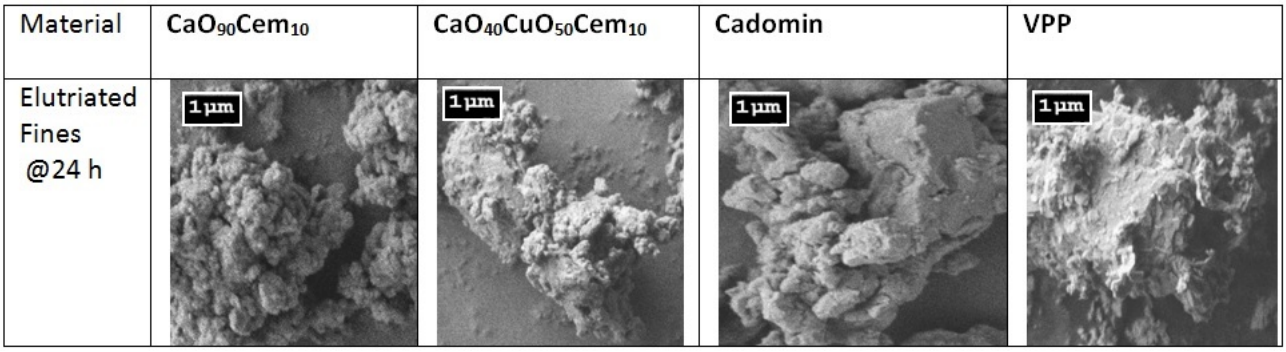

Figure 4.9 SEM images of elutriated fines of $CaO_{10}CuO_{10}cem_{10}$, $CaO_{90}cem_{10}$, cadomin and VPP catalyst at 500 °C after 24 h. The fines from $CaO_{10}CuO_{10}cem_{10}$ and cadomin appear agglomerated.

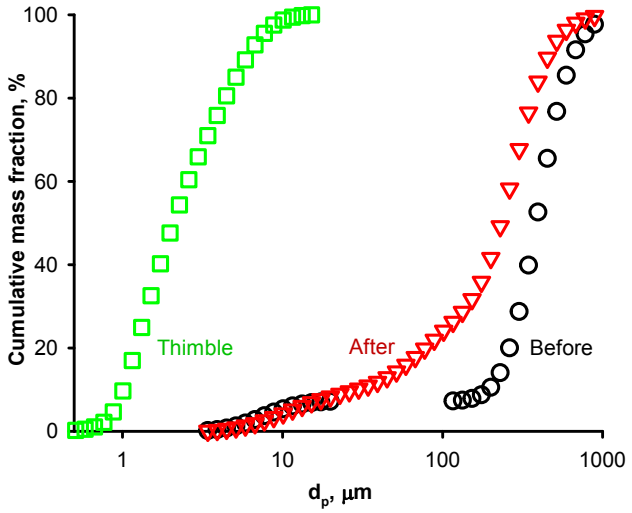

Figure 4.10 The cadmonin elutriated fines were finer than all other powders we tested. The cadomin before the attrition test and powder recovered from the jet cup had 7 % –20 µm.

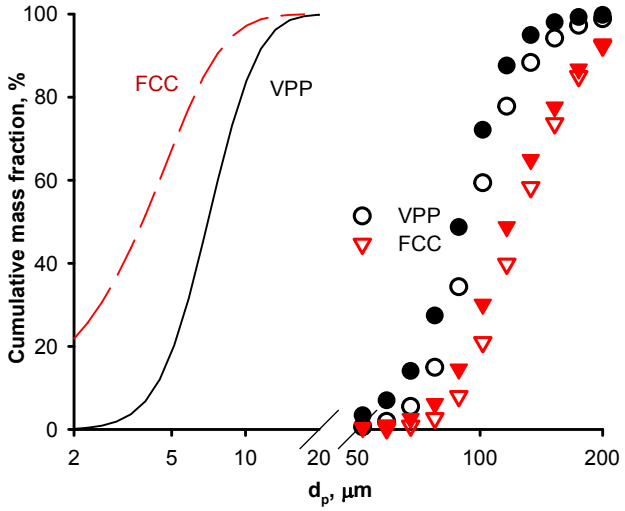

Figure 4.11 The hollow symbols represent the PSD of VPP and FCC before the test and the full symbols are the PSD after the test. The FCC elutriated fines are much finer than the VPP but no particles are greater than 20 µm.

circulated for several years at 400 °C with very low solids losses.

4.6 Mechanism

Gas jets are major source of attrition in fluidized beds. Poorly distributed gas promotes gulf streaming, bypassing and low conversion yields. To distribute gas uniformly across the reactor requires a grid pressure drop as much as 30 % of the bed pressure drop. Consequently, the orifice velocity exceed 100 m s^{-1} and even the velocities exiting the sparger shrouds approach

Table 4.3 The sorbent attrition rate decreases with increasing temperature.

Powder	T °C	BET m^2 g^{-1}	Pore volume cm^3 g^{-1}	d_{50} µm	$R_{a,j}$ mg h^{-1}
$CaO_{40}CuO_{50}cem_10$	23	13	0.2	310	26
$CaO_{40}CuO_{50}cem_10$	500	15	0.2	330	19
$CaO_{40}CuO_{50}cem_10$	800	12	0.2	422	19
$CaO_{90}cem_{10}$	23	16	0.5	384	21
$CaO_{90}cem_{10}$	500	18	0.5	263	33
$CaO_{90}cem_{10}$	800	19	0.5	300	50

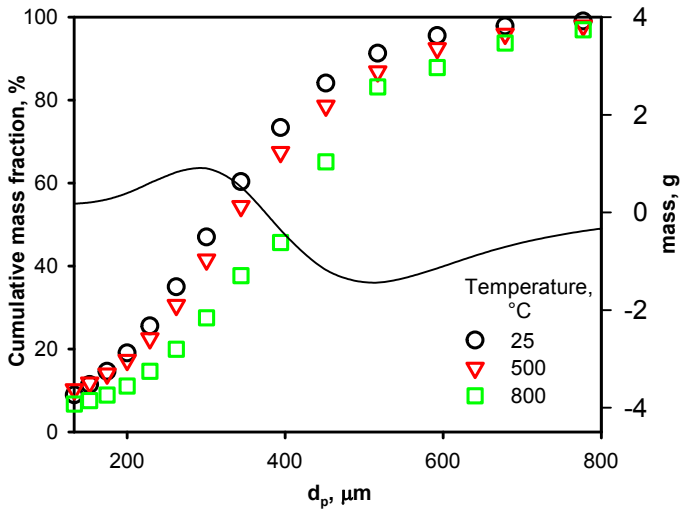

Figure 4.12 Both the attrition rate and the fragmentation rate of $CaO_{90}cem_{10}$ increases with temperature. The +400 µm mother particles form as many –200 µm particles as +200 µm –400 µm.

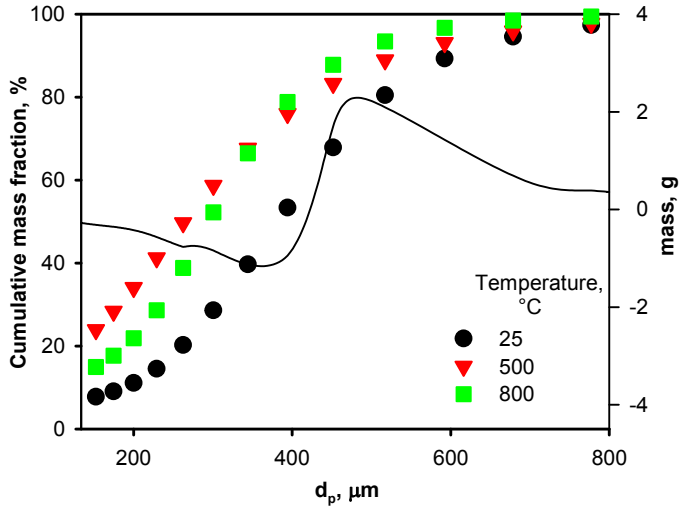

Figure 4.13 The attrition rate of $CaO_{40}CuO_{50}cem_{10}$ increases with temperature but the +200 µm –400 µm particles agglomerate. An equal mass of +200 µm –400 µm particles disappear as +400 µm form. While the d_{50} increases from 310 µm to 420 µm, the d_{sv} decreases from 260 µm to 240 µm because of the larger fraction of -200 µm.

this velocity.

Attrition rates depend on material properties — particle size, surface structure, shape, density and porosity — and process conditions — gas and solids velocity, wall hardness, solids residence time, system temperature and pressure [73]. Accelerated attrition tests guide the catalyst design process and indicate the amount of binder required to achieve mechanical stability suitable for fluidized beds [31].

High orifice velocity induce attrition; and attrition rates increase to the third power with respect to the orifice velocity. Maximizing pressure drop will distribute the gas best but will induce high attrition rates. Low grid pressure drop results in poor reactor performance as the gas will preferentially enter one side of the bed and create large solid eddies.

The particle become more rounded with time as surface asperities cleave. In DuPont's CFB reactor to produce maleic anhydride from n-butane, during the first 80 d of operation, the Sauter mean particle diameter increased from 45 µm to 50 µm (Fig. 4.14). Thereafter it remained essentially constant. The cyclone velocities in fluidized bed acrylonitrile processes are much higher than in the the DuPont's CFB reactor [74]. Consequently, attrition rates, due to abrasion, are higher and catalyst must be continually added to the reactor to maintain the fines fraction ($20\,\mu m < d_p < 44\,\mu m$) greater than 30 %. When the fines fraction drops below this level, the acrylonitrile yield drops.

Cyclones are designed to maintain greater than 99.99 % of particles greater than 20 µm. Most asperities that cleave from the surface of particles are smaller and the cyclones are unable to maintain them in the reactor. Consequently, the particle size will only change slightly with time since the surface asperities contribute little to the average particle size distribution.

On the other hand, the PSD of catalyst that fragments may change measurably. In this case, the size of the daughter particles are on the same order of magnitude as the mother particles. The cyclones will be able to maintain these particles in the bed and the PSD will become smaller with time. However, because the fragments have irregular shapes, their attrition resistance is poorer. The may fragment more frequently or become rounded more readily than the mother particle (abrasion).

Core-in-shell catalyst (VPP[109]) are manufactured by spray drying micron sized powders (1 µm to 2 µm) with nano size silica that forms a resistant outer shell. When core-in-shell catalyst attrit they form both large fragments (pieces of the shell) and many small particles. The cyclones are unable to retain the small particles (less than 10 µm and the shell fragments attrit rapidly as well. Thus with time on stream the PSD become essentially constant, which is consistent with the DuPont PSD data (Fig. 4.14) [49, 74].

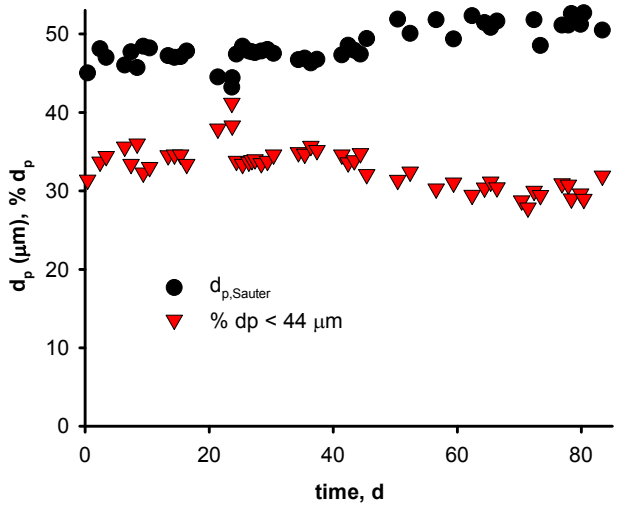

Figure 4.14 Fresh VPP particle size distribution during the first 83 d of operation in DuPont's Circulating Fluidized Bed reactor [49].

Attrition rate correlations in jet mills [56] are different than in large scale equipment [107]. The advantage of jet mills is that they require as little as 20 g of solids, which makes them convenient for screening. Furthermore, gas density, velocity, orifice diameter and particle size can be studied independently. Large scale units require substantial amounts of solids and the data are confounded; they might provide better data to project to larger scale performance but it is more difficult to identify the contribution of individual factors. Here, we compare the attrition resistance of novel sorbents with catalyst — VPP and FCC — that are well characterized and operate in similar reactor hydrodynamic conditions.

4.6.1 Orifice velocity

Attrition increases with orifice velocity raised to a power of 3 in jet mills [56] and in fluidized beds the power approaches 4 [107]. In our tests, at velocities ranging from $180\,\mathrm{m\,s^{-1}}$ to $230\,\mathrm{m\,s^{-1}}$, the best fit value of the exponent approaches 4 (Fig. 4.15), which agrees with previous work [57]. Attrition rates increased from $5\,\mathrm{mg\,h^{-1}}$ to $14\,\mathrm{mg\,h^{-1}}$, $8\,\mathrm{mg\,h^{-1}}$ to $21\,\mathrm{mg\,h^{-1}}$ and $10\,\mathrm{mg\,h^{-1}}$ to $26\,\mathrm{mg\,h^{-1}}$ for VPP, FCC and $CaO_{40}CuO_{50}cem_{10}$ respectively as jet velocity increased. The attrition rate of the VPP is low because it had been in the commercial CFB reactor for several years and thus only mechanically resistant powder remained.

We expressed attrition rate as a function of normalized factors of gas velocity, density and orifice diameter (Eq. 4.8). The gas velocity was normalized with respect to sonic velocity of

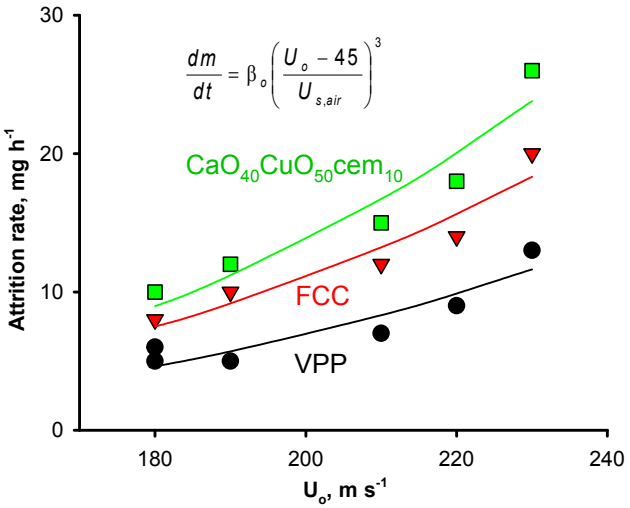

Figure 4.15 The attrition rate depends on gas velocity raised to a power. For a value of β_1 =4, best fit value for $U_c = 0$, for a value of β_1 =3, $U_c = 50\,\mathrm{m\,s^{-1}}$ and for a value of $\beta_1 = 2$, $U_c = 100\,\mathrm{m\,s^{-1}}$.

air, U_s, gas density with respect to air at 25 °C and orifice diameter normalized with respect to 0.39 mm.

$$\frac{dm}{dt} = \beta_o \left(\frac{U_g - U_c}{U_s}\right)^{\beta_1} \left(\frac{\rho_g}{\rho_{air}}\right)^{\beta_2} \left(\frac{d_o}{0.39}\right)^{\beta_3} \tag{4.8}$$

We introduce a critical velocity, U_c, below which attrition is negligible. This parameter introduces an extra degree of freedom such that there are multiple parameters that fit the experimental data equally well (Table 4.4). A critical velocity of zero fits the data best when the exponent is assigned a value of 4; it is about $50\,\mathrm{m\,s^{-1}}$ with an exponent of 3; and, it approaches $100\,\mathrm{m\,s^{-1}}$ with an exponent of 2. Concurrently with increasing the order on the the normalized gas velocity (β_1), the value of (β_0) also increases.

Small orifices are necessary to maintain a high pressure drop across the grid to distribute gas uniformly. Shrouds are necessary to reduce the velocity of the gases entering the bed to minimize the gas velocity at the nozzle to minimize attrition. DuPont's CFB had 531 orifices in the grid for which the shroud velocity reached $80\,\mathrm{m\,s^{-1}}$. It had 1862 angled oxygen spargers in which the gas velocity exceeded $100\,\mathrm{m\,s^{-1}}$. Despite these high velocities, the attrition rates in the plant were less than $1\,\mathrm{kg\,h^{-1}}$.

Introducing a critical velocity changes the relationship between attrition rate and pressure

Table 4.4 Best fit parameters for the attrition rate as a function of velocity based on Eq. 4.8. The critical velocity increases with a decreasing value of the exponent. All three expressions fit the experimental data equally well.

Exponent of U_g	β_0		
	$\beta_1 = 2$	$\beta_1 = 3$	$\beta_1 = 4$
	U_c =95	U_c=45	U_c=0
$CaO_{40}CuO_{50}cem_{10}$	32	50	71
FCC	20	30	50
VPP	12	13	24

— gas density. Nozzles operate at gas velocities close to the critical velocity. Increasing the pressure drop while maintaining the gas velocity constant increases the attrition rate proportionately, according to Eq. 4.4. According to Eq. 4.8, when the orifice (or nozzle) velocity is below a critical velocity, the attrition rate is independent of pressure: this relationship implies that, increasing pressure will increase attrition rate but proportionally less than expected verses a linear relationship with gas density.

We ignored the quantity of catalyst that the thimble collected during the first 6 h (6 h dump) when we calculated the attrition rate. The initial attrition rate of VPP at $180\,\mathrm{m\,s^{-1}}$ was $5\,\mathrm{mg\,h^{-1}}$ whereas those of fresh FCC and $CaO_{10}CuO_{10}cem_{10}$ were $12\,\mathrm{mg\,h^{-1}}$ and $14\,\mathrm{mg\,h^{-1}}$, respectively (Fig. 4.16).

4.6.2 Gas density

High temperature reduces gas density but standard powders attrition rate is measured at ambient temperature. Increasing temperature to assess $R_{a,j}$ confounds several effects: gas density, viscosity, momentum and the effect temperature may have on the particle morphology (sintering, for example). To isolate the effect of density from temperature (and morphological changes), we tested CO_2, He and air on $CaO_{40}CuO_{50}cem_{10}$, FCC and VPP catalyst. We expected that the attrition rate would increase linearly with the molecular weight of the gas but a power law model with an exponent of 0.41 characterized the data best ($R^2 = 0.960$) (Fig. 4.17). The model fit was somewhat poorer when we assigned and a value of 0.5 to the exponent ($R^2 = 0.947$) but it was unacceptable with an exponent of 1 ($R^2 = 0.700$). The values of the coefficient (β_o) are 28, 24 and 13 for $CaO_{40}CuO_{50}cem_{10}$, FCC and CPP catalyst respectively.

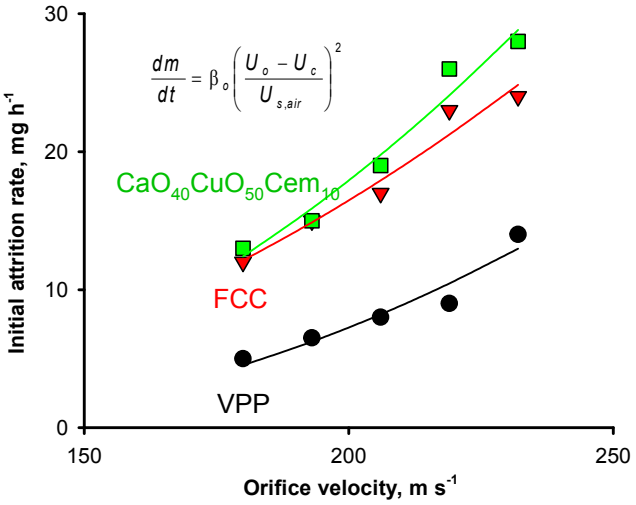

Figure 4.16 The initial attrition rate of (during the first 6 h $CaO_{10}CuO_{10}cem_{10}$, and fresh FCC are double that of equilibrated VPP at all gas velocities.

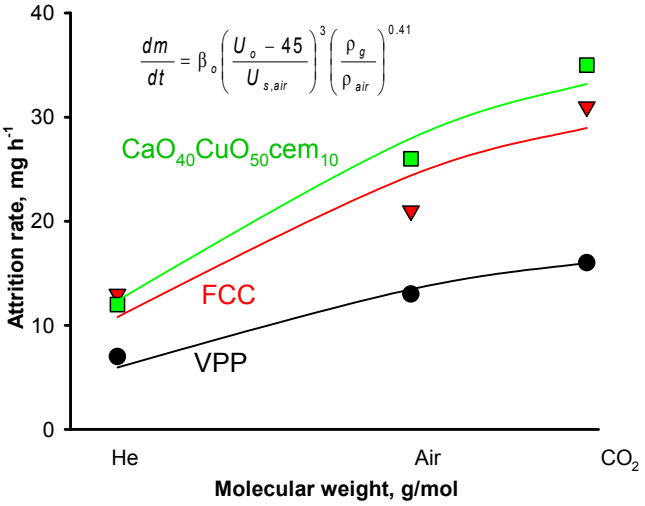

Figure 4.17 Effect of gas molecular weight on attrition rate. The effect of gas density (molecular weight) and viscosity are confounded. The attrition rates correlates with the inverse square root of gas density.

Table 4.5 Eq. 4.8 normalizes all factors to standard conditions. Therefore, the parameter β_o should be invariant. It is constant for the $CaO_{40}CuO_{50}cem_{10}$, FCC and VPP

Test condition	$CaO_{40}CuO_{50}cem_{10}$	FCC	VPP
U_g	45	36	23
d_o	45	39	24
M	49	43	24

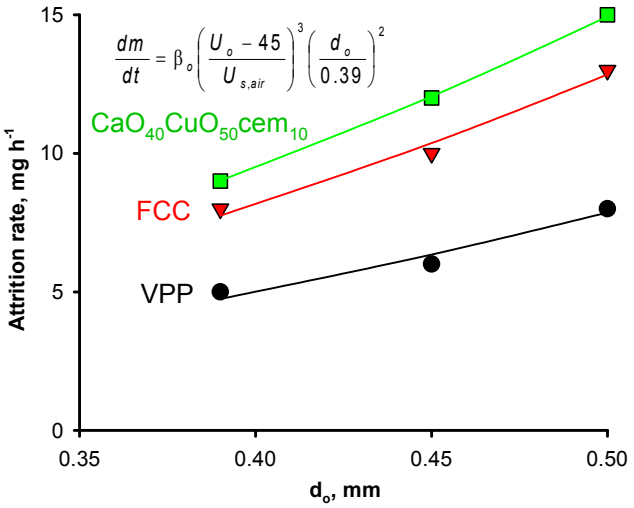

Figure 4.18 Effect of orifice diameter on attrition rate. The attrition rate of catalyst and sorbent increased with orifice diameter squared.

4.6.3 Orifice diameter

The orifice diameter and number of sparers determines what the pressure drop across the grid or sparger manifold will be. Although the gas velocity exiting the shroud will be the determining factor for attrition, studying the orifice diameter should confirm its effect. We tested three diameters: 0.39 mm, 0.45 mm, and 0.5 mm. $R_{a,j}$ increases with the square of the orifice diameter. The model accounts for 99 % variance in the data (Fig.4.18). The second order dependency agrees with Werther's relationship (Eq.4.4). At the same gas velocity, the mass of gas will increase proportionately with the surface area. The mass of gas induces more collisions between the particles and, as a consequence, increases the attrition rate.

4.7 Conclusion

A major inconvenience of fluidized beds versus fixed beds for catalytic processes relates to fine management and particle attrition. Operating spargers at low gas velocity minimizes attrition rates but at the expense of distributing gas uniformly across the vessel. Attrition rates of sorbents and catalysts increase with the product of gas mass flow rate and orifice velocity. It also increases with orifice diameter and approximately with the square root of the gas density.

Of the CaL sorbents we tested, $Ca_{90}cem_{10}$ had the highest attrition resistance at low temperature but was more susceptible to attrit at 800 °C compared to $CaO_{40}CuO_{50}cem_{10}$. In fact, the latter agglomerated at about 800 °C: the +200 µm –400 µm powder formed +400 µm powder. The attrition rates of the sorbents were double that of VPP catalyst but equivalent to the FCC powder at ambient conditions. The attrition rates might be unacceptably high at 800 °C but adding more cement may resolve the poor high temperature performance.

The attrition mill predominantly measures surface abrasion (and shattering). We estimated fragmentation rates by comparing the particle size distribution of the powder recovered in the jet mill with the PSD before the attrition test. Fragmentation rates are an order of magnitude larger than attrition rates in during the first 24 h in the mill but after 96 h these rates are only twice as high.

Manganese could potentially replace copper as the oxidant since it has a higher melting temperature and thus better stability. Future work should concentrate on assessing the sorbents mechanical stability while cycling between carbonation and calcination.

Acknowledgements

Project funding from Carbon Management Canada is gratefully acknowledged. The authors also thank Prof. Arturo Macchi of University of Ottawa for his exemplary project leadership and Natural Resources Canada for providing the sorbents. Provision of VPP catalyst from E. I. du Pont de Nemours and Company is duly acknowledged.

Nomenclature

cem	cement
R	Attrition rate
K	Attrition rate constant
M	Mass
U	Velocity
x	Mass fraction
ρ	density
μ	viscosity
ξ	voidage

Subscripts

c	cyclone
j	jet
mf	minimum fluidization
sv	surface volume
i	particle size class
o	orifice
g	gas
p	particle

CHAPTER 5 GENERAL DISCUSSION

Integration of calcium looping and chemical looping combustion is a technology that holds great prospect for pre and post combustion capture of CO_2. Calcium looping requires an expensive air separation unit which increases cost of capturing CO_2. Integrated CaL−CLC avoids the air separation unit. Fluidised bed combustions are the reactors of choice in commercial CaL-CLC. The problem of particle attrition hinder their effective use. Other advantages of the proposed sorbent include:

1. Gaseous fuels such as CH_4 can be employed instead of the convectional solid fuels. This reduces the quantity of solids to be pumped round and hence savings in energy consumption.

2. Prevention of corrosive carbon dioxide stream from combustion of solid fuels due to presence of oxygen and sulphur.

3. Exothermic oxidation of Cu during sorbent regeneration process can be used to generate electricity.

The concept behind this work achieves two goals:

1. Capture of CO_2 and

2. Generation of electricity.

This thesis has explored the possibility of using an attrition resistant novel calcium aluminate bound Cao−CuO−cement sorbent for post- combustion CO_2 capture. We have designed jet mill attrition testing system for low temperature test. High temperature attrition test is critical in assessing the attrition resistance of the sorbents. We adapted the jet mill for high attrition test.

$Ca_{90}Cem_{10}$ had the highest resistance to attrition at low temperature but loss of material almost doubled when the temperature was raised to 800 °C. $Ca_{40}CuO_{50}Cem_{10}$ agglomerated at about 800 °C which resulted in defluidization. This caused reduction in the rate of fines production. It, however, did not sinter. This is interesting since copper which caused agglomeration can be replaced with with a more agglomeration resistant oxygen carrier such as manganese. Considering the fact that jet velocities used in this studies were from $180\,\mathrm{m\,s^{-1}}$ to $230\,\mathrm{m\,s^{-1}}$, which are not expected in industrial fluidized bed combustors, sorbent $Ca_{90}Cem_{10}$

and $Ca_{40}CuO_{50}Cem_{10}$ will be suitable for commercialization purposes if agglomeration related issues with sorbent $Ca_{40}CuO_{50}Cem_{10}$ are overcome.

Calcination almost doubled the loss of material from the sorbents. Composition of sorbent had significant effect on attrition resistance. At low temperature, the two main materials of interest: $Ca_{90}Cem_{10}$ and $Ca_{40}CuO_{50}Cem_{10}$ have attrition resistance which is almost of the same order of magnitude as that that of fresh FCC but both of them must be recomposed to make them more resistant to attrition. The inclusion of 10 % cement increased the attrition resistance by 50 % compared to natural cadomin limestone. Attrition rates of sorbents and catalysts increase with the product of gas mass flow rate and almost fourth power of orifice velocity. It also increases with square of orifice diameter and approximately with the square root of the gas density.

Sorbent attrition occurred mainly due to fragmentation. PSD of fines generated mainly by abrasion did not change during the course of the test suggesting that mode of sorbent attrition did not changes.

CHAPTER 6 CONCLUSION

6.1 Advancement of knowledge

Integrated calcium looping and chemical looping combustion is a promising technology for post-combustion CO_2 capture in dual fluidized bed combustors. A metal oxide supplies the needed oxygen thus avoiding the need for an expensive air separation unit. Sorbent attrition is a major concern. In this work, we utilized a novel sorbent that overcomes problems associated with individual disadvantages of of CaL and CLC. Three groups of factors: operating parameters, material properties and design parameters that are likely to affect loss of Ca-based sorbent in calcium looping processes have been investigated. Major outcome of this work include:

1. Design of attrition test protocol which is valid for high temperature (800 °C) jet mill attrition test.
2. Distinction between the modes of attrition and fragmentation rate through particle size distribution analysis.
3. Development of a correlation to predict the attrition rate of sorbent in jet mills.

6.2 Limits and constraints

The main challenge of this project was gas leakages at high temperature and orifice plugging. This was solved by designing a gas injection system with gas preheating to avoid heating the jet cup to 800 °C.

6.3 Recommendations

The following are recommended for future work

1. Typical integrated calcium looping and chemical looping combustion process involves multiple cycling; which has the tendency to increase sorbent attrition. Simulation of sorbent attrition during cycling should be studied by cycling the sorbent while fluidising the sorbent with different gases at reactive conditions.
2. The choice of oxygen carrier can have an effect on the attrition resistance of the sorbent. Selection of oxygen carrier that give optimum performance (attrition resistance) of the

sorbent should be conducted by performing attrition resistance studies of the oxygen carriers with the same attrition testing setup.

3. Agglomeration and sintering effects can be avoided by replacing copper with manganese. The homogeneous composition has not achieved its desired purpose and new method of fabricating the core-in-shell sorbent must be explored. The VPP catalyst is a clear indication that the core- in-shell composition must be the way forward.

4. We need to install a series of pre-heaters to raise the temperature of gas before delivering to the jet cup.

BIBLIOGRAPHY

[1] I.E.A. International energy agency, "CO_2 emissions from fuel combustion highlights", (2014).

[2] D. Zingaretti, G. Costa, and R. Baciocchi, "Assessment of the energy requirements for CO_2 storage by carbonation of industrial residues. Part 1: Definition of the process layout", Energy Procedia, vol. 37, 2013, pp. 5850 – 5857.

[3] E. J. Wilson, T. L. Johnson, and D. W. Keith, "Regulating the ultimate sink:managing the risks of geologic CO_2 storage", Environmental Science Technology, vol. 37, 2003, pp. 3476-3483.

[4] H. Yang, Z. Xu, M. Fan, R. Gupta, R. B. Slimane, A. E. Bland, and I. Wright, "Progress in carbon dioxide separation and capture: A review", Journal of Environmental Sciences, vol. 20, 2008, pp. 14-27.

[5] A. C. Backham, L. Croiset, and E. Douglas, Simulation of CO_2 capture using MEA scrubbing: A flow sheet decomposition method, Energy Conversion and Management, vol. 46, 2005 , pp. 475- 487.

[6] D. Singh, E. Croiset, P.L. Douglas, and M.A. Douglas, "Techno-economic study of CO_2 capture from an existing coal-fired power plant: MEA scrubbing vs. O_2-CO_2 recycle combustion", Energy Conversion and Management, vol. 44, 2003, pp. 3073-3091.

[7] J. C Abanades, E. J. Anthony, D. Y. Lu, C. Salvador, and D. Alvarez, "Capture of CO_2 from combustion gases in a fluidized bed of CaO", J. AIChE vol. 50, 2004 pp. 1614-22.

[8] J. C. Abanades, G. Grasa, M. Alonso, N. Rodriguez, E. J. Anthony, and L. M. Romeo, "Cost structure of a post-combustion CO_2 capture system Using CaO", Environmental Science and Technology, vol. 41, 2007, pp. 5523-5527.

[9] F. Yu, N. Phalak, Z. Sun, and L. Fan, "Activation strategies for calcium based sorbents for CO_2 capture: a perspective", Industrial and Engineering Chemistry Research, vol. 51, 2012, pp. 2133-2142.

[10] M. V. Iyer, H. Gupta, B. B. Sakadjian, and L. Fan, "Multi-cyclic study on the simultaneous carbonation and sulfation of high-reactivity CaO" Industrial and Engineering Chemistry Research, vol. 43, 2004, pp. 3939-3947.

[11] B. R. Stanmore, and P. Gilot, "Review- calcination and carbonation of limestone during thermal cycling for CO_2 sequestration", Fuel Processing Technology, vol. 86, 2005, pp. 1707-1743.

[12] V. Manovic, and E. J. Anthony, "Integration of calcium and chemical looping combustion using composite CaO/CuO-based materials", Environmental Science and Technology, vol. 45, 2011 pp. 10750-10756.

[13] M. Hossain, and H. de Lasa, "Chemical looping combustion for inherent CO_2 capture separations-a review", Chemical Engineering Science, vol. 63, 2008, pp. 4433-4451.

[14] P. Cho, T. Mattison, and A. Lyfelt, "Comparison of iron, copper, and manganese-based oxygen carriers for chemical looping combustion", Fuel, vol. 83, 2004, pp. 1215-1225.

[15] B. Metz, O. Davidson, H. C. de Coninck, M. and L. A. Meyer, : "IPCC Special Report on carbon dioxide capture and storage, Prepared by working group III of the intergovernmental panel on climate", Cambridge University Press, Cambridge, United Kingdom and New York, NY, USA, 2005.

[16] V. Manovic, and E. J. Anthony, "Ca-based pellets with oxygen carriers and catalysts", Energy & Fuels, vol. 25, 2011, pp. 4846-4853.

[17] J. Adanez, L. F, de Diego, F. Garcia-Labiano N. P. Gaya, and A. Abad, "Selection of oxygen carriers for chemical-looping combustion", Energy & Fuels, vol. 18, 2004 , pp. 371-377.

[18] J. Blamey, E. J. Anthony, J. Wang, and P. S. Fennel, "Calcium looping cycle for large scale CO_2 capture", Progress in Energy and Combustion Science, vol. 36, 2010, pp. 260-279.

[19] T. Shimizu, T. Hirama, H. Hosoda, K. Kitano, M. Inagaki and K. Tejima, "A twin fluid-bed reactor for removal of CO_2 from combustion processes", Chemical Engineering Research and Design, vol. 77, 1999, pp. 62-68.

[20] A. Charitos, C. Hawthorne, A. R. Bidue, S. Sivalingam, A. Schuster, H. Spliethoff and Q. Scheffkrecht, "Parametric investigation of the calcium looping process for CO_2 capture in a 10 kWth dual fluidized bed", International Journal Greenhouse Gas Control, vol. 4, 2010, pp. 776-784.

[21] N. Rodriguez, M. Alonso, G. Grasa and J. C. Abanades, "Heat requirements in a calciner of $CaCO_3$ integrated in a CO_2 capture system using CaO", Chemical Engineering Journal, vol. 138, 2008, pp. 148-154.

[22] D. Y. Lu, R. W. Hughes, and E. J . Anthony, "Ca-based sorbent looping combustion for CO_2 capture in pilot-scale dual fluidized beds, Fuel Process Technology, vol. 89, 2008, pp. 1386-1395.

[23] V. Manovic Wu Y. He, and E. J. Anthony, "Core-in-shell CaO/CuO-based composite for CO_2 capture", Industrial and Engineering Chemistry Research, vol 50, 2011, pp. 12384-12391.

[24] G. S. Patience, and P. L. Mills, "Modelling of propylene oxidation in a circulating fluidized-bed reactor", Studies in Surface Science and Catalysis, vol. 82, 1994, pp. 1-18.

[25] J. Werther, "Scale-up modelling for fluidized bed reactors", Chemical Engineering Science, 47 (1992), 2457-2462.

[26] R. Boerefijn, N. J. Gudde, and M. Ghadiri, "A review of attrition of fluid cracking catalyst particles", Advanced Powder Technology, vol. 11, 2000, pp. 145-174.

[27] R. P. Davuluri, and T. M. Knowlton, "Development of a standardized attrition test procedure", In:L. S. Fan, T. M. Knowlton, (Eds). Fluidization IX. New York: Engineering Foundation, 1998, pp. 333-340.

[28] W. G. Vaux, and D. L. Keairns, "Particle attrition in fluid bed processes", In: Fluidization, J. R. Grace and J. M. Matsen (Eds), Engineering Foundation, New York, 1980, pp. 445- 452.

[29] J. Werther, and J. Reppenhagen, In: W. C. Yang(Ed),"Attrition" Handbook of fluidization and fluid particle systems attrition, Mercel Dekker, 2003, pp. 211-217.

[30] G. Xiao, J. R. Grace, and C. J. Lim, "Attrition characteristics and mechanism for limestone particles in an air-jet apparatus", Powder Technology, vol. 207, 2011, pp. 183-191.

[31] V. Materic, R. Holt, M. Hyland, and M. I. Jones, "An internally circulating fluid bed for attrition testing of Ca Looping sorbents", Fuel, vol. 127, 2014, pp. 116-123.

[32] C. R. Bemrose, and J. Bridgewater, "A review of attrition and attrition test methods", Powder Technology, vol. 49, 1987, pp. 97-126.

[33] J. E. Gwyn, "On the particle size distribution function and attrition of cracking catalysts", AIChE Journal, vol. 15, 1969, pp. 35-39.

[34] B. Epstein, "Logarithmic-normal distribution in breakage of solids". Industrial and Engineering Chemistry Research, vol. 41, 1948, pp. 2289-2291.

[35] A. Kokkkoris, and R. Turton, "A phenomenological model predicting the attrition and the reduction of attrition due to the addition of solid lubricants in slugging beds", Powder Technology, vol. 84, 1995, pp. 39-47.

[36] L. Jia, R. Hughes, D. Lu, E. J. Anthony, and I. Lau, "Attrition of calcining limestones in circulating fluidised bed systems", Industrial Engineering Chemistry Research, vol. 46, 2007, pp. 5199-5209.

[37] W. L. Forsythe Jr. and W. R. Hertwig, "Attrition characteristics of fluid cracking catalysts —laboratory studies", Industrial and Engineering Chemistry Research, vol. 41, 1949, pp. 1200-1206.

[38] A. U. Neil, and J. Bridgewater, "Towards a parameter characterising attrition", Powder Technology, vol. 106, 1999, pp. 37-44.

[39] ASTM. "American standard testing method, D5757, Standard test methods for determination of attrition of FCC catalysts by air jets", 2011.

[40] A. Knight, N. Ellis, J. R. Grace, and C. J. Lim, "CO_2 sorbent attrition testing for fluidized bed systems", Powder Technology, vol. 266, 2014, pp. 412–423.

[41] ASTM, "American standard testing method, D409M, standard test method for grindability of coal by hardgrove-machine method", 2011.

[42] F. C. Bond, Crushing and grinding calculations", Part II, British Chemical Engineering, vol. 6, 1961, pp. 378-385.

[43] R. Cocco, Y. Arrington, R. Hays, J. Findlay, S. B. R. Karri, and T. M. Knowlton, "Jet cup attrition testing", Powder Technology, vol. 200, 2010, pp. 224-233.

[44] J. Tomczek, P. Mocek, Attrition of coal ash particles in a fluidized bed, AIChE Journal, vol. 53, 2007, pp. 39-46.

[45] A. Thom, and J. Werther, "Attrition resistance of a VPO catalyst", Applied catalysis A: General, vol. 376, 2010, pp. 56-65.

[46] J. Rappenhegen, J. Werther, "Catalyst attrition in cyclones", Powder Technology, vol. 113, 2000, 55-69.

[47] M. Pell, "Gas fluidization". In: Handbook of Powder Technology, Amsterdam: Elsevier, 1990, pp. 97-106.

[48] R. M. Contractor, H. E. Bergna, U. Chowdhry, and A. W. Sleight, "Attrition resistant catalysts for fluidized bed-systems", In: J.R, Grace, L. W. Shemilt, M.A. Bergougnou, Eds, Fluidization VI, New York, Engineering Foundation, 1989, pp. 589-596.

[49] G. S. Patience, and R. E. Bockrath, "Butane oxidation process development in a circulating fluidized bed", Applied Catalysis A: General vol. 376, 2010, pp. 4-12.

[50] G. Xiao, J. R. Grace, and C. J. Lim, "Limestone particle attrition in high-velocity air jets", Industrial and Engineering Chemistry Research, vol. 51, 2012, pp. 556-560

[51] B .R. Sereshki, S. J. Balan, G. S. Patience, and J. L. Dubois, "Reactive vaporisation of crude glycerol in a fluidised bed reactor", Industrial and Engineering Chemistry Research, vol. 49, 2010, pp. 1050-1056.

[52] F. Scala, and P. Salatino, "Flue gas desulfurization under simulated oxyfiring fluidised bed combustion conditions: The influence of limestone attrition and fragmentation", Chemical Engineering Science, vol. 65, 2010, pp. 556-561

[53] F. Scala, and P. Salatino , "Limestone fragmentation and attrition, during fluidised bed oxyfiring", Fuel, vol. 89, 2010, pp. 827-832 .

[54] S. F. Wu, and M. Z. Jiang, "Formation of a $Ca_{12}AL_{14}O_{33}$ nanolayer and its effect on the attrition behaviour of CO-adsorbent microspheres composed of CaO nanoparticles", Industrial and Engineering Chemistry Research, vol. 49, 2010, pp. 12269-12275 .

[55] G. Xiao, J. R. Grace, and C. J. Lim, "Evolution of limestone particle size distribution in an air-jet attrition apparatus", Industrial and Engineering Chemistry Research, vol. 53, pp. 2014, pp. 15845-15851.

[56] J. Werther, W. Xi, Jet attrition of catalyst particles in gas fluidised beds", Powder Technolgy, vol. 76, 1993, pp. 39-46

[57] M. Ghadiri, J. A. S. Cleaver, and V. G. Tuponogov, J. Werther, "Attrition of FCC powder in the jetting region of a fluidised bed", Powder Technology, vol. 80, 1994, pp. 175-178.

[58] M. Ryden, P. Moldenhauer, S. Lindqvist, T. Mattisson and A. Lyngfelt, "Measuring attrition resistance of oxygen carrier particles for chemical looping combustion with a customized jet cup", Powder Technology, vol. 256, 2014, pp. 75-86.

[59] R. Zhao, J. G. Goodwin, K. Jothimurugesa, J. Spivey, and S. k. Gangwal, "Comparison of attrition test methods; ASTM standard fluidised bed vs Jet Cup", Industrial and Engineering Chemistry Research, vol. 39, 2000, pp. 1155-1158.

[60] L. Cairati, L. D. Fiore, P. Forzatti, and I. F. Trifiro, "Oxidation of methanol in a fluidized bed. 1. Catalyst attrition resistance and process variable study", Ind. Eng. Chemical Process Development, vol. 19, 1980, pp. 561-565.

[61] C. L. Lin, and M. Y. Wey, "Influence of hydrodynamic parameters on particle attrition during fluidization at high temperature", Korean Journal of Chemical Engineering, vol. 22, 2005, pp. 154-160.

[62] S. H. Lee, S. D. Kim, and D. H. Lim, "Particle size reduction of anthracite coals during de-volatilization in a thermo-balance reactor", Fuel, vol. 81, 2002, pp. 1633-1639.

[63] H. Chen, C. Zhao, Y. Yang,and P. Zhang, "CO_2 capture and attrition performance of CaO pellets with aluminate cement under pressurized carbonation", Applied Energy, vol. 91, 2012, pp. 334-340.

[64] B. Gonzalez, M. Alonso, and J. C. Abanades, "Sorbent attrition in a carbonation/calcinations pilot plant for capturing CO_2 flue gases", Fuel, vol. 89, 2010, pp. 2918-2924.

[65] Z. Chen, J. R. Grace, and C. J. Lim, "Limestone particle attrition and size distribution in a small circulating fluidised bed", Fuel, vol. 87, 2008, pp. 1360-1371.

[66] M. Broda, A. M. Kierzkowska, and C. R. Muller, "Influence of the calcination and carbonation conditions on the CO_2 uptake of synthetic Ca-based CO_2 sorbents", Environmental science Technology, vol. 46, 2012, pp. 10849- 10856.

[67] Y. Wu, V. Manovic, I. He and E. J. Anthony, "Modified lime-based pellet sorbents for high temperature: reactivity and attrition behavior", Fuel, vol. 96, 2012, pp. 454-461.

[68] R. Pacciani, C. R. Muller, J. F. Davidson, J. .S. Dennis, and A. N. Dennis, "Synthetic Ca-based solid sorbents suitable for capturing CO_2 in a fluidized bed", Canadian Journal of Chemical Engineering, vol. 86, 2008, pp. 356-366.

[69] Q. Changlei, d. Hong, L. Liang. Y. Junjun, F. Bo, "CO_2 capture performance and attrition property of CaO-Based pellets manufactured from organometallic calcium precursors by extrusion", Energy & Fuels, vol, 28, 2014, pp. 329-339.

[70] P. S . Fennell, R. Pacciani, J. S. Dennis, J. F. , Davidson, A. N. Hayhurst, "The effects of repeated cycles of calcination and carbonation on a variety of different limestones, as measured in a hot fluidized bed of sand", Energy & Fuels, vol. 21, 2007, pp. 2072-2081.

[71] D. Y. Lu , R. W. and Hughes, E. J. Anthony, "Ca-based sorbent looping combustion for CO_2 capture in pilot-scale dual fluidized beds", Fuel Processing Technology, vol. 89, 2008, pp. 1386-1395.

[72] J. J. Pis, A. B. Fuertes, V. Artos, and A. Suarez, "Attrition of coal and ash particles in a fluidized bed". Powder Technology, vol. 66, 1991, pp. 41-46.

[73] W. Xi, "Catalyst attrition in fluidized bed systems", PhD dissertation, Technical University Hamburg-Harburg, 1993.

[74] A. Thon A. Puttmann, E. Hartge, S. Henrich, J. Werther, G.S. Patience, and R.E.Bockrath, "Simulation of catalyst loss from an industrial reactor on the basis of lab-scale attrition test", Powder Technology, vol. 214, 201l, pp. 21-30 .

[75] A. Thon, and J. Werther, "Attrition resistance of a VPO catalyst", Applied catalysis A: General, vol. 376, 2010, pp. 56-65.

[76] J. Reppenhagen, and J. Werther, "Catalyst attrition in cyclones", Powder Technology, vol. 113, 2000, pp. 55-69.

[77] F. Scala, F. Montagnaro, and P. Salatino, "Attrition of limestone by impact loading in fluidised beds", Energy & fuels, vol. 21, 2007, pp. 2566-2572.

[78] Z. Chen, C.J. Lim, J. R. Grace, "Development of particle size distribution during limestone impact attrition", Powder Technology, vol. 207, 2011, pp. 55-64.

[79] Z. Chen, C. J. Lim, and J. R. Grace, "Study of limestone particle impact attrition", Chemical Engineering Science, vol. 62, 2007, pp. 867-877.

[80] ASTM. "American standard testing method, D7743-12, Standard test method for measuring the minimum fluidization velocities of free flowing powders", 2012.

[81] D. Kunii, and O. Levenspiel, Fluidization Engineering, Butterworths, Boston, 1991.

[82] P. H. Shipway, and I. M. Hutchings, "Attrition of brittle spheres by fracture under compression and impact loading", Powder Technolology, vol. 76, 1993, pp. 23-30.

[83] H. Wadell, "Sphericity and roundness of rock particles, Journal of Geology, vol. 41, 1933, pp. 310-331.

[84] P. Chen, C. I. Sishtla, D. V. Punwani , and H. Arastoopour, "A model for attrition in fluidized beds", In: Fluidization, J. R. Grace and J. M. Matsen (Eds),Engineering Foundation, New York, 1980, pp. 445- 452.

[85] T. P. Ponomareva, S. I. Kontorovich, and E. D. Shchukin, "Attrition of spherical racking catalysts in the presence of powdered lubricants", Kinetics and Catalysis, vol. 21, 1980, pp. 397- 401.

[86] D. Geldart, "Types of gas fluidization, Powder technol., vol. 7, 1973, pp. 285-292.

[87] J. R. Grace, Contacting modes and behaviour classification of gas—solid and other two-phase suspensions" Canadian Journal of Chemical Engineering, vol. 64, 1986, pp. 353.

[88] W. R. A. Goossens, "Classification of fluidized particles by Archimedes number", Powder Technology, vol. 98, 1998, pp. 48-53.

[89] O. Molerus, "Interpretation of Geldart's type A, B, C and D powders by taking into account interparticle cohesion forces" Powder Technology, vol. 33, 1982, pp. 81-87.

[90] W. Yang, "Modification and re-interpretation of Geldart's classification of powders", Powder Technology, vol. 171, 2007, pp. 69-74.

[91] D.M. Bachovchin, J.M. Beer , and A. F. Sarofim, "Investigation into the steady-state elutriation of fines from a fluidized bed", AIChE Symp. Ser., vol. 205, 1981, pp. 76.

[92] R. Chirone, M. D'Amore, L. Massimila, and A. Mazza, "Char attrition during the batch fluidized bed combustion of coal" AIChE Journal, vol. 31, 1985 , pp. 812-820.

[93] J. Choi, J. Suh, In. Chang , D. Shun, C. Yi, J. Son, and S. Kim, "The effect of fine particles on elutriation of coarse particles in a gas fluidized bed", Powder Technology, vol. 121, 2001, pp. 190-194.

[94] J. M. D. Merry, "Penetration of vertical jets into fluidized beds", AIChE J. vol. 21, 1957, pp. 507-510.

[95] F. A. Zenz, "Bubble formation and grid design". Inst. Chem. Eng. Symp. Ser., vol. 30, 1968, pp. 136-145.

[96] C. Y. Wen, M. Horio, R. Krishnan, R. Kosravi,and P. Rengarajan, "Jetting phenomena and dead zone formation on fluidized bed distributors", Proc. Second Pacific Chemical Engineering Congress, Denver, Colorado, vol. 2, 1977, pp. 1182.

[97] F. V. J. Benjeloun, "In Determination des longueurs de jets de gaz horizontaux dans des lits fluidises, textes des communications presentees a l'occasion des 6emes journées europeenenes" sur la fluidisation, Toulouse, Laguerie, C. G., P., Ed. Toulouse, 1991.

[98] J. Li and K. Kato, "Effect of electrostatic and capillary forces on the elutriation of fine particles from a fluidized bed", Advanced Powder technology, vol. 12, 2001, pp. 187-205.

[99] J. Li and K. Kato, "Effect of cohesive powders on the elutriation of particles from a fluid bed", Chemical Engineering Science, vol. 59, 2004, pp. 2777-2782.

[100] W. C. Yang, and D. L. Keairns, "Design and operating parameters for a fluidized bed agglomerating combustor/gasifier", In: fluidization , Davidson JR, Keairns DL, (Eds)., Cambridge: Cambridge University Press, 1978, pp. 208-214.

[101] S. B. R. Karri, and Grid Design, PSRI Design Manual, 1994.

[102] R. H. Perry, and W. D. Green, Perry's chemical engineering' handbook, 8th edition, McGraw-Hill: New York, 2008.

[103] T. M. Knowton and I Hirsan In: Grace JR, Matsen JM, eds. Fluidization, Plenum Press, 1980, pp. 315.

[104] "National Oceanic & Atmospheric Administration , Full Mauna Loa CO_2 record", 2014 http://www.esrl.noaa.gov/gmd/ccgg/trends.

[105] L-S Fan, L. Zeng, W. Wang, and S Luo, "Chemical looping processes for CO_2 capture and carbonaceous fuel conversion–prospect and opportunity", Energy & Environmental Science, vol. 5, 2012, pp. 7254–7280.

[106] C. Alie, L. Backham, E. Croiset,and P. L. Douglas, "Simulation of CO_2 capture using MEA scrubbing: a flowsheet decomposition method", Energy Conversion and Management, vol.46, 2005, pp. 475–487.

[107] J. McMillan, C. Briens, and F. Berruti Ed. Chan, "Particle attrition mechanism with a sonic gas jet injected into a fluidized bed", Chemical Engineering Science, vol. 62, 2007, pp. 3809—3820.

[108] V. Manovic, and E. J. Anthony, "Screening of binders for pelletization of CaO-based sorbents for CO_2 capture", Energy & Fuel, vol. 23, 2009, pp. 4797–4804.

[109] R. M. Contractor, D. I. Garnett, H. S. Horowitz, H. E. Bergna G. S. Patience, J. T. Schwartz, and G. M. Sisler, "A new commercial scale process for n-butane oxidation to

maleic anhydride using a circulating fluidized bed reactor", Studies in Surface Science and Catalysis, vol. 82, 1994, pp. 233–242.